24

Influence of Global Warming on the RC Structures and Durability Monitoring in Civil Engineering

Guofu Qiao et al.*
School of Civil Engineering
Harbin Institute of Technology, Harbin
China

1. Introduction

Global warming has or will affect all aspects of human life on Earth. We will focus on the influence of global warming in civil engineering and the structural health monitoring (SHM) technologies here. Obviously, reinforcing concrete (RC) structures are the most important structural style in civil engineering. With the development of global warming and further deterioration of the environment, the conditions of RC structures now becomes more atrocious than that of before. In the past few decades, many tremendous bridges, skyscrapers, super dams and other huge harbor works have been built. These structures are expected to serve safely for tens of years to hundreds of years. Unfortunately, the corrosion of the reinforcing steel, called as "cancer of the steel", has been a world-wide problem which deteriorates the durability of RC structures and degrades the serviceability severely. The corrosion of RC structures has resulted in very high repair costs, which sometimes are even much greater than the initial construction cost, and in some extreme situations, leaded to collapse of the structure. The corrosion of the reinforcing steel in concrete will then be a fatal attack to the durability of RC structures. Fortunately, structural health monitoring systems enable scientists and engineers to identify the status of structures, and then provide the foundation for safety assessment, service-life prediction, maintenance & reinforcement and full-life design of structures.

2. Mechanism of the reinforcing steel's corrosion

Generally, the hydrated reactions of the cement can be shown as Eq. (1) to Eq. (7). As the hydration reaction of cement is completed, the cement should been changed into a complex multi-phase and heterogeneous body[1]. Hydration product normally provides a high

* Tiejun Liu[2], Guodong Sun[3], Yi Hong[4], Baoguo Han[1], Huigang Xiao[1], Zhichun Zhang[4] Jinping Ou[1,5]
[1]*School of Civil Engineering, Harbin Institute of Technology, Harbin, China*
[2]*Shenzhen Graduate School, Harbin Institute of Technology, Shenzhen, China*
[3]*Department of Computer Science and Technology, Tsinghua University, Beijing, China*
[4]*Center for Composite Material and Structure, Harbin Institute of Technology, Harbin, China*
[5]*School of Civil & Hydraulic Engineering, Dalian University of Technology, Dalian, China*

$$2C_3S + 11H \rightarrow C_3S_2H_8 + 3CH \quad (1)$$

$$2C_2S + 9H \rightarrow C_3S_2H_8 + CH \quad (2)$$

$$C_3A + 3C\bar{S}H_2 + 26H \rightarrow C_6A\bar{S}_3H_{32} \quad (3)$$

$$2C_3A + C_6A\bar{S}_3H_{32} + 4H \rightarrow 3C_4A\bar{S}H_{12} \quad (4)$$

$$C_4A\bar{S}H_{12} + 2C\bar{S}H_2 + 16H \rightarrow C_6A\bar{S}_3H_{32} \quad (5)$$

$$C_4AF + 3C\bar{S}H_2 + 21H \rightarrow C_6(A,F)\overline{\bar{S}_3}H_{32} + (F,A)H_3 \quad (6)$$

$$C_4AF + C_6(A,F)\overline{\bar{S}_3}H_{32} + 7H \rightarrow 3C_4(A,F)\bar{S}H_{12} + (F,A)H_3 \quad (7)$$

degree of protection to the reinforcing steel against corrosion, by virtue of the high alkalinity (CH , PH > 13.5) of the pore solution. Under high alkalinity, steel remains passivated. The basic factors and fundamental corrosion processes of the reinforcing steel's corrosion are illustrated as Fig.1. When the pH value of the pore solution drops to low values due to the carbonation reaction $Ca(OH)_2 + CO_2 + H_2O \rightarrow Ca(HCO_3)_2 + CaCO_3$ or as sufficient chloride ions penetrate into the reinforcement, the protective film is destroyed and the reinforcing steel is depassivated. Furthermore, corrosion in the form of rust formation and loss in cross-section of the rebar occur in the presence of oxygen and water (humidity).

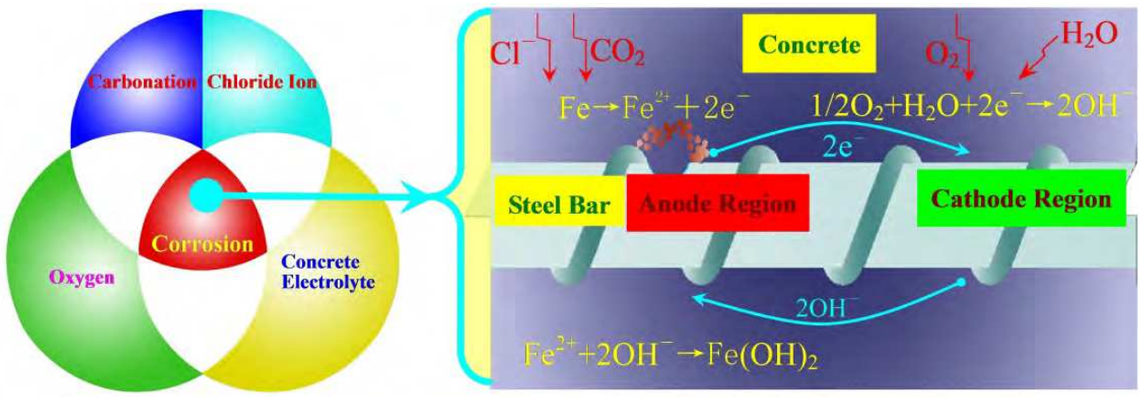

Fig. 1. Schematic plan of the reinforcing steel's corrosion process in concrete

Essentially, the corrosion process is an electrochemical reaction process. CO_2 and Cl^- often lead to general corrosion and pitting corrosion, respectively. During the general corrosion process, Fe atom is oxidized to $Fe(OH)_2$, Fe_3O_4, $Fe(OH)_3$ or $Fe_2O_3 \cdot nH_2O$ at the anode region.

The oxidation state depends on the content of O2 in the concrete. On the other hand, O atom at the cathode region is reduced to O^{2-}.The micro anode and cathode on the surface of the reinforcing steel form the microcell. Compared with that of the general corrosion, the pitting corrosion process is much more complicated. It is generally agreed that the barrier oxide layer of the metal is a highly defective structure, with the point defects being metal and oxygen vacancies and metal interstitials. Macdonald has developed a point model (PDM) to descript the growth and breakdown of passive films[2]. The fundamental basis of the general PDM is illustrated in Fig.2, in which the basic reactions that lead to the generation and annihilation of point defects at the interfaces (Reactions (1)-(6)), together with film dissolution (Reaction (7)), are displayed.

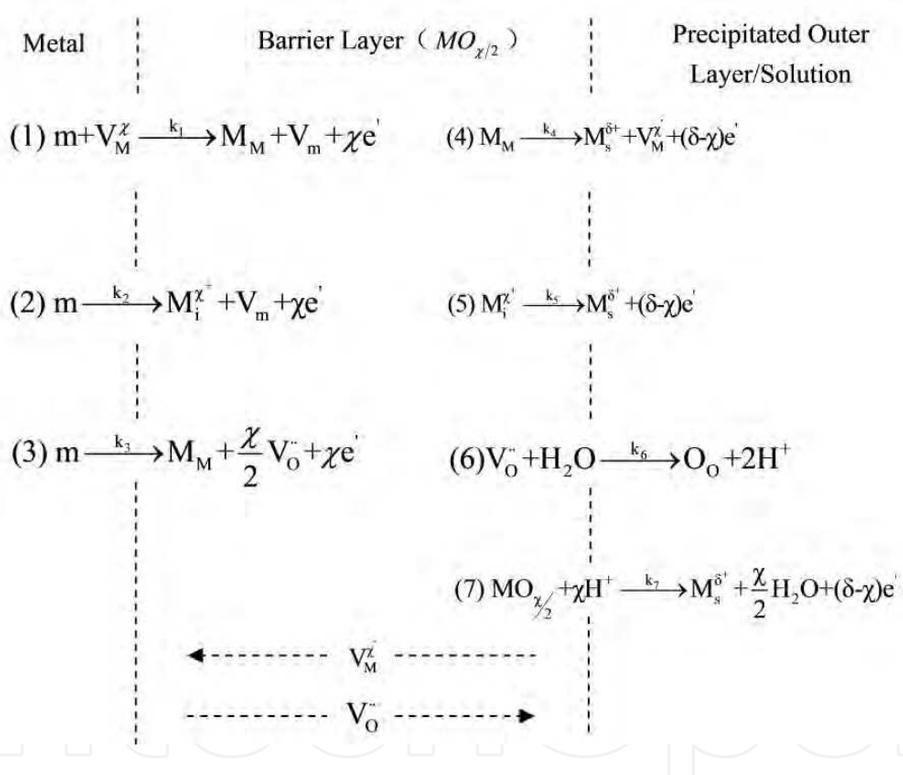

Fig. 2. Schematic of physico-chemical processes that occur within a passive film according to the Point Defect Model

According to D.Macdonald's PDM, the anion Cl^- is able to enhance the flux of cation vacancies through the barrier layer, such that under favorable conditions (voltage, PH, $[Cl^-]$) vacancy condensation will occur at the metal/barrier layer interface and hence passivity breakdown will ensue. The initial reaction occurring at the film/solution interface is the absorption of an aggressive anion (Cl^-) into a surface oxygen vacancy followed by a Schottky-pair-type reaction. Anion absorption leads to the generation of cation vacancies at

the film/solution interface and, hence, to the flux of cation vacancies across the passive film to the film/metal interface. If the cation vacancy diffusivity is so high that the flux of cation vacancies can not be accommodated by that of cations generated at the metal/film interface, a cation vacancy condensate will be formed, causing the local thinning of the film or detachment from the metal. Once the condensate has grown to a critical size, the film ruptures and hence a rapid local attack occurs, either due to complete dissolution or else to the stress in the film that induces a mechanical or structural instability. The postulated reactions of the aggressive anions Cl- in this process are illustrated in Fig.3.

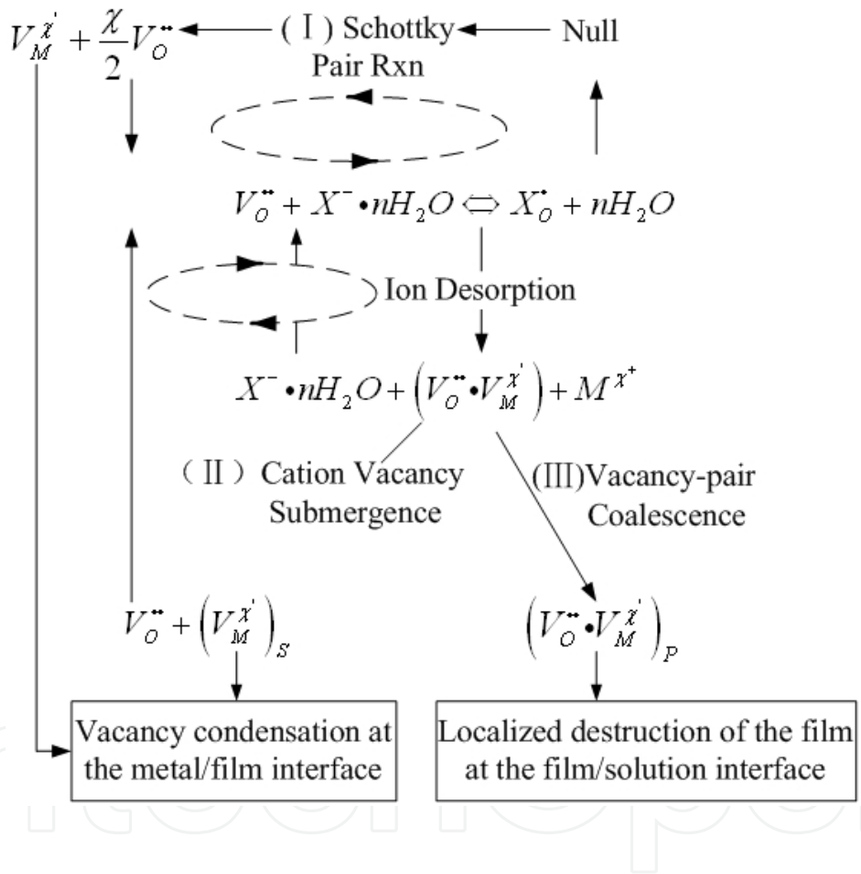

Fig. 3. Postulated reactions for cation vacancy generation at the barrier layer/solution interface according to the Point Defect Model

Although the general corrosion and the pitting corrosion process are very complicate, it must keep in mind that the electron is presented and transferred inside the barrier layer or on the surface of the reinforcing steel. The energy from the steel-smelting process is delivered by the electrochemical reactions and physicochemical processes described above. Furthermore, this delivered energy will be applied as the power source of the self-powered wireless corrosion monitoring sensor in future.

3. Characterize the corrosion by the EIS and EN techniques

3.1 Review of the electrochemical measurement techniques

Equivalent circuit (EC) is the transfer function of the electrochemical system. The EC in Fig.4 is the universal transfer function which can be used to simulate and characterize the electrochemical characteristics of the steel-concrete system[3,4].

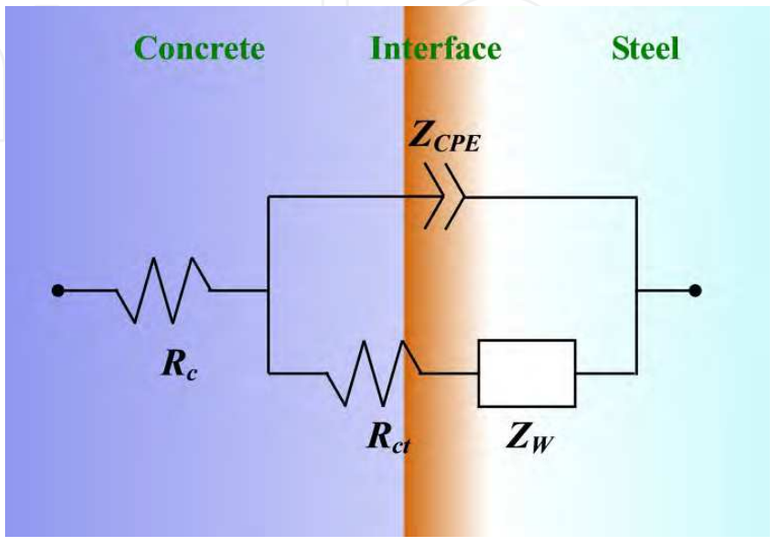

Fig. 4. EC of steel-concrete system.R_c, R_{ct}, Z_W and Z_{CPE} are the resistance of concrete, Faraday resistance, impedance of the diffusion process and the impedance of CPE, respectively.

R_c and R_{ct} are the resistance of the concrete and reactive resistance of the corrosion, respectively. Z_W and Z_{CPE} represent the diffusion impedance of oxygen and dispersion impedance of the concrete-steel interface, respectively. The diffusion of the oxygen results in the Warburg impedance. Z_w can be calculated as follows:

$$Z_w = \frac{1}{Y_{0W}}(j\omega)^{-\frac{1}{2}} = \frac{\sigma}{\sqrt{\omega}} - j\frac{\sigma}{\sqrt{\omega}} \tag{8}$$

Where σ is the Warburg coefficient. Y_{0W} is the admittance as follows,

$$Y_{0W} = \frac{nFC_s\sqrt{D}}{\gamma Z_F^0 |I_F|} \tag{9}$$

Where Z_F^0 is Faraday impedance without diffusing effect, γ is the reaction order of the reactant; I_F is the faradic current; n, F are the constants, C_s is the concentration at electrode's surface. The coarse interface of the steel-concrete, isolated reaction region and the heterogeneous nature of concrete are the most important factors causing the dispersion effect. This phenomenon is depicted by the constant phase element (CPE). The CPE is expressed as Eq. (10) by IUPAC.

$$Z_{CPE} = \frac{1}{Y_{0dl}}(j\omega)^{-n} = \frac{1}{Y_{0dl}}\omega^{-n}\left(\cos\frac{n\pi}{2} - j\sin\frac{n\pi}{2}\right) \tag{10}$$

Where Y_{0dl} is basic admittance and n is the constant in the region (0, 1],

$$Y_{0dl} = \frac{\omega^{-n}}{|Z_{CPE}|} \tag{11}$$

The dispersion effect and the diffusion of the oxygen can prolong the balance time of the electrochemical system, or even lead the system never to reach the balance state. According to the results of V.Feliu, J.A.Gonzalez and C.Andrade[3,4], dispersion effect and diffusion effect can influence the response of the excitation of galvanostatic step at initial time region and long term region, respectively. Therefore, the parameters of R_c, R_{ct} and Z_{CPE} can be extract accurately by fitting the experimental results at initial time region. Applying the experimental results at long term region, Z_W can also be calculated. Once the elements in the EC are calculated, the corrosion characteristics of the concrete-steel system can be clarified.

The electrochemical corrosion status of the steel-concrete system can be recognized by active monitoring technique (AMT) and passive monitoring technique (PMT). As the EC in Fig.4 is the universal transfer function for general corrosion, abundantly actuating signals can be applied to excite the concrete-steel system in linear region or nonlinear region. Therefore, the electrochemical elements which include R_c, R_{ct}, Z_W and Z_{CPE} can be extracted in time domain or frequency domain by analyzing the responses of the concrete-steel system to these actuating signals. Table 1 listed the major AMTs which are applied extensively in corrosion measurement. For the pitting corrosion which is caused by Cl^-, electrochemical emission spectrum (EES) in PMTs is the most effective technique to recognize the corrosion status of the reinforcing steel. Essentially, electrochemical noise (EN) reflects the intrinsic information of the initial, metastable, repassive and stable stages during the pitting corrosion process. Listening passively to the reinforcing steel confides how the corrosive mediums intrude the RC structures, the pitting corrosion status can be identified. Many methods have been developed to analyze the EN data in time domain[5], frequency domain[6] or in chaos domain[7]. Wavelet transform (WT) has been proposed as an alternative tool to overcome the limitations of FFT in the analysis of non-stationary signals of the EN data. It can provide the information on transients in time domain and the possibility of working with non-stationary signals. The previous research has shown that It is much better to decompose the EN data during the pitting process of the reinforcing steel to wavelet space, and extract the characteristics of the EN based on WT much more effectively[8].

AMT	Actuating Signal	Response Signal
Electrochemical Impedance Spectrum(EIS)	Current/Voltage	Voltage/Current
Electrochemical Frequency Modulation(EFM)	Current/Voltage	Voltage/Current
Harmonic Analysis(HA)	Current/Voltage	Voltage/Current
Transient Galvanostatic Decay	Current	Voltage
Transient Potentiostatic Decay	Voltage	Current
Potentialdynamic Scan	Voltage	Current
Linear Polarization	Current/Voltage	Voltage/Current
Coulostatic Method	Electric Charge	Voltage/Current

Table 1. AMTs in corrosion measurement

Electrochemical Impedance Spectrum(EIS) technique has been widely used as a corrosion measurement tool. A number of publications have reviewed both the theory and many areas of application [9-12]. These reviews suggest that AC impedance is a useful technique for determining mechanistic and kinetic information about the corrosion processes occurring at corroding interfaces. The experimental impedance data $Z(j\omega)_{exp}$ may be well approximated by the impedance $Z(j\omega)_{equiv}$ of an equivalent circuit made up of ideal resistors, capacitors, inductors and various distributed elements. In such a circuit, elements represent the various processes involved in the transport of charge and mass in the system being investigated. Various equivalent circuits have been proposed to explain the impedance response of film-covered surfaces, which involve cathodic and anodic reactions in the system. In the last few decades, many researchers [13, 14] have done lots of work about steel corrosion. By extracting the information from the high, medium and low frequency region of EIS, many qualitative and quantitative parameters about electrochemical process of carbon steel in cement mortar can be gotten. The corrosion process of carbon steel in cement mortar can be reflected by these parameters.

Electrochemical noise (EN) technique has been widely used to study the corrosion process of various metallic materials, such as metals [15, 16] and organic coated metals [17, 18], and it can provide useful information about the corrosion mechanism by measuring the fluctuations of the current and potential simultaneously, which are generated during the corrosion process. One of the advantages of electrochemical noise technique is that it does not conduct any disturbing signal. Therefore it is able to avoid the artificial disturbances to the system during the measurement [19]. The sensitivity of EN measurement is much higher than that of the other traditional techniques to the localized corrosion process [20]. Many methods have been developed to analyze the EN data [21], including statistical analysis [22, 23] and spectral analysis [24-26]. However, the most commonly-used EN analysis methods (statistical and spectral) mentioned above are devised for stationary signals that do not show distinctive transients .The main disadvantage of those methods is that they analyze signals by averaging the features across the whole time record [27]. DC trend removal method is another problem which obstacles the application of ENA in practical engineering.

Wavelet transform (WT) has been proposed as an alternative tool to overcome the limitations of FFT in the analysis of non-stationary signals of EN data [28, 29]. It can provide the information on transients in time and the possibility of working with non-stationary signals, so it has been used to differentiate corrosion type and to study corrosion mechanism of process [30, 31]. Only some work of EN for studying the corrosion of reinforcing steel in concrete has been reported [32, 33]. A. Legat[33] found that the electrochemical noise technique was able to follow the high corrosion dynamics in concrete, and the measured signals containing certain fluctuations indicated that the process of corrosion initiation consisted of a sequence of several events. Their results of the measurements also revealed that the distribution of anodic and cathodic sites could alternate during the wetting and drying of concrete. Hu et al. [34] studied the corrosion behavior of reinforced steel in the simulated concrete pore solution by using electrochemical noise, and they analyzed the EN data by discrete wavelet and provided a criterion to determine the threshold value controlling the turning of corrosion state of steel in concrete. The aim of this work is to study the corrosion process of reinforcing steel in cement mortar and illustrate the fact that the EDP is an effective indicator of the pitting corrosion in corrosion monitoring

3.2 EIS Performance of the RC system

Three-electrode system has been used in the experiment. The working electrode is Q235 carbon steel which is widely used in civil engineering. The specimens are embedded in epoxy resin. Working electrode's surface is polished with 400,800, 1200 and 2000 grit silicon carbide paper and cleaned with ethanol and acetone. Its working area is 1.13cm^2. When steel corrosion in concrete is studied by EN, the carbon steel specimen is embedded in cement mortar (Fig.5).When EIS is measured, one of the two identical working electrodes is substituted for graphite electrode. The mass ratio of sand, cement and water is 3:1:0.6. SCE reference electrode is used to measure potential.

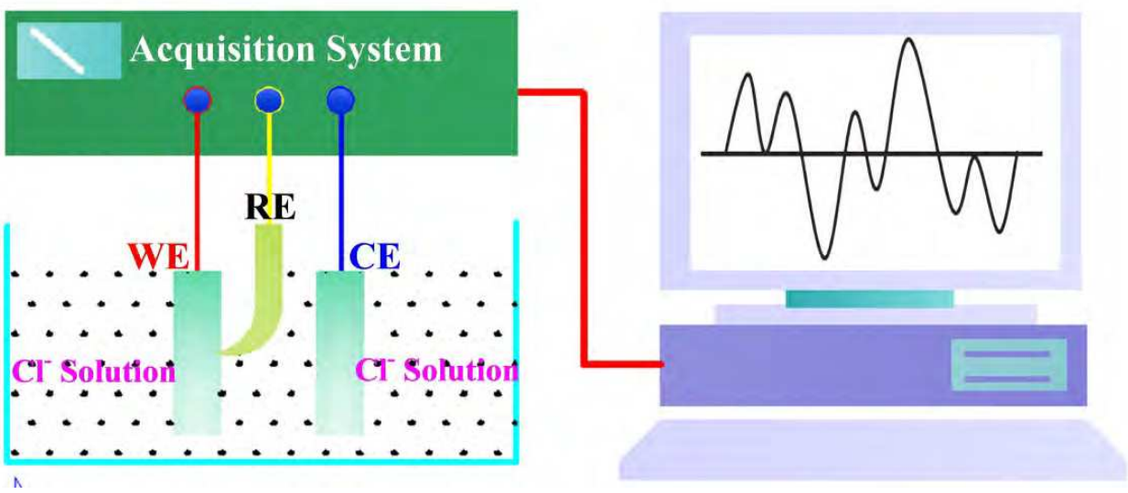

Fig. 5. Schematic plan of the three-electrode electrochemical measurement system

Two kinds of influencing factors which are temperature and concentration of NaCl solution are considered during the experiment. EN is measured under the condition that the temperature is 50℃ and the concentration of NaCl solution is 3.0%. The sampling frequency is 2Hz. As temperature and concentration of NaCl solution is changed from 26℃ to 50℃ and 0.5% to 5.0%, respectively, EIS is measured. Princeton Applied Research Potentiostat/Galvanostat Model 263A is used. The frequency range of EIS measurement is 10^5Hz to 10^{-3}Hz. In order to accelerate the seepage velocity of NaCl solution to the steel bar surface in concrete, all the cement mortar specimens are put into the pressure pan. We have kept the pressure of the span at 7MPa for 60mins by the pressure pump before unloading it. Then all the specimens are immersed in different concentration of NaCl solution for 70days.

The Nyquist plots at 26℃ and 50℃ are shown in Fig.6., Fig.7 and Fig.8 show the Bode plotsat 26℃ and 50℃, respectively[8]. Concentration of sodium chloride solution changes from 0.5% to 1.0%, 3.0% and 5.0%. From the Nyquist and Bode plots we can see that there are two pieces of capacitive impedance arc. The capacitive impedance arcs at high frequency (from 10^5Hz to 10^3Hz) are generated by the sodium chloride solution outside the cement mortar layer. The resistance of the solution is no more than a few hundred Ohms. The other capacitive impedance arcs are caused by the cement layer. The equivalent circuit (EC) of cement layer is composed of resistance element R_c and capacitive element C_c. Obviously, the capacitive impedance arc has been flattened in the medium frequency region (between KHz to 100mHz). This phenomenon is often caused by CPE. Smearing phenomenon has arisen at the low frequency region.

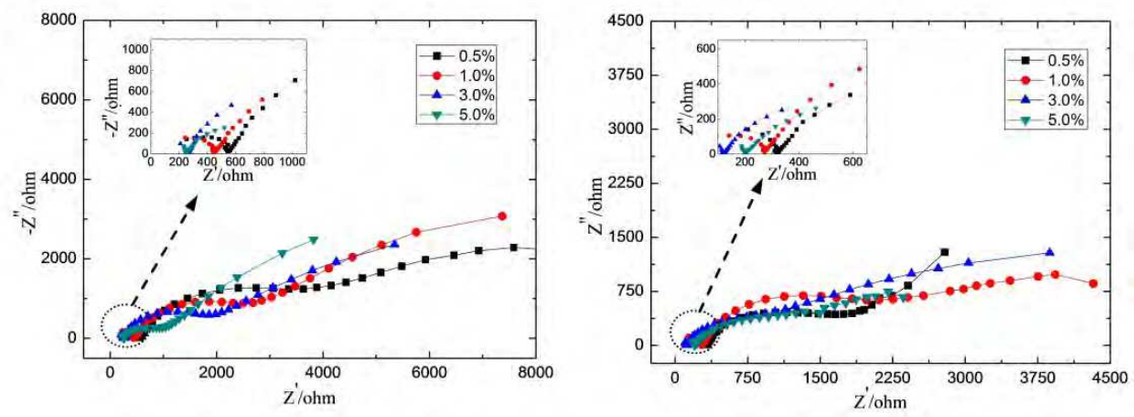

(a) 26°C (b) 50°C

Fig. 6. Nyquist plots of Q235 carbon steel in cement mortar with different NaCl solution

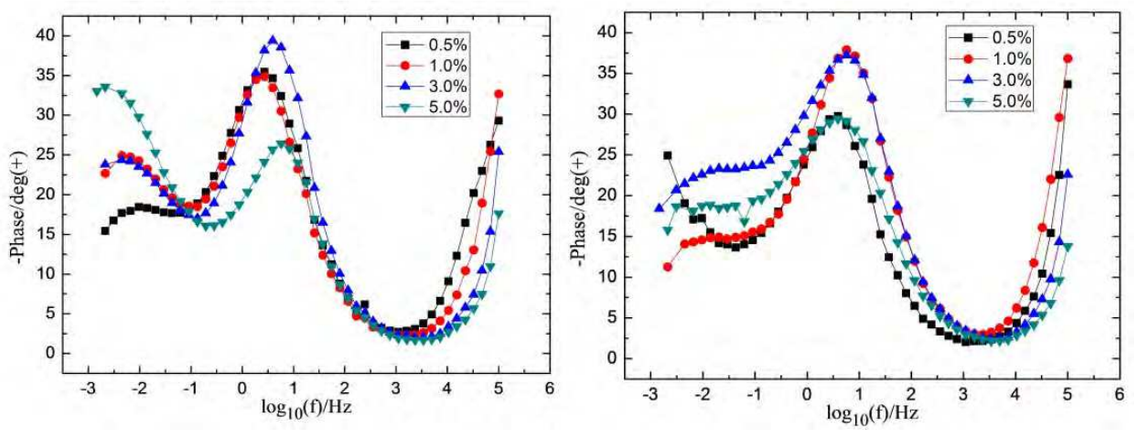

(a) 26°C (b) 50°C

Fig. 7. Bode plots of Q235 carbon steel in cement mortar with different NaCl solution

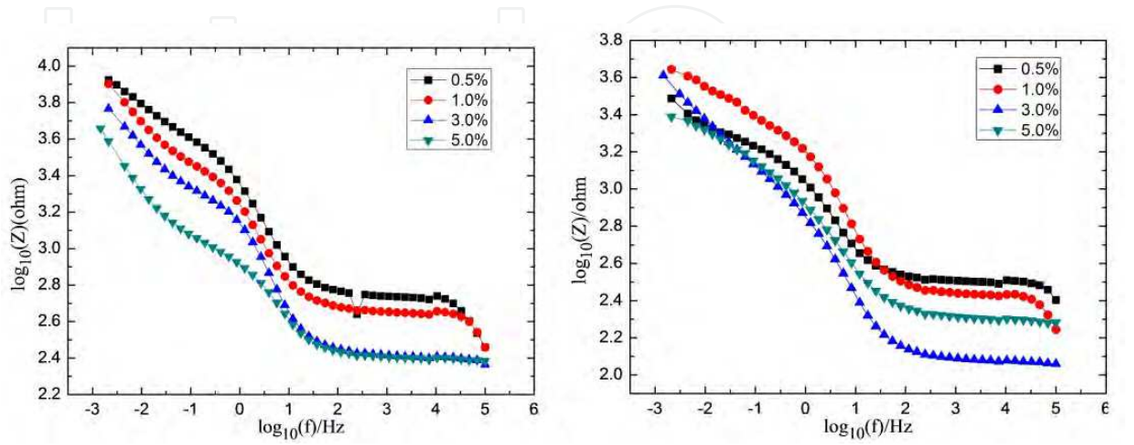

(a) 26°C (b) 50°C

Fig. 8. Impedance-frequency plots of Q235 carbon steel immersed in different NaCl solution

According to the Nyquist and Bode plots feature, the much more detailed EC in Fig.9 is used to simulate the Q235 carbon steel corrosion in the cement mortar. R_{sol} is the resistance of chloride sodium solution. R_c and C_c are the resistance and capacity of cement layer respectively. Because there exists smearing phenomenon in the Nyquist plots, Warburg impedance exists in the electrochemical process. W represents the diffusing effect of Oxygen. Q represents the dispersion effect. By fitting the experiment results with the EC in Fig. 7 by ZSimpWin3.20 software, we can obtain the value of the parameters in the EC. The fitting results of 26℃ and 50℃ are listed in Table 2 and Table 3, respectively.

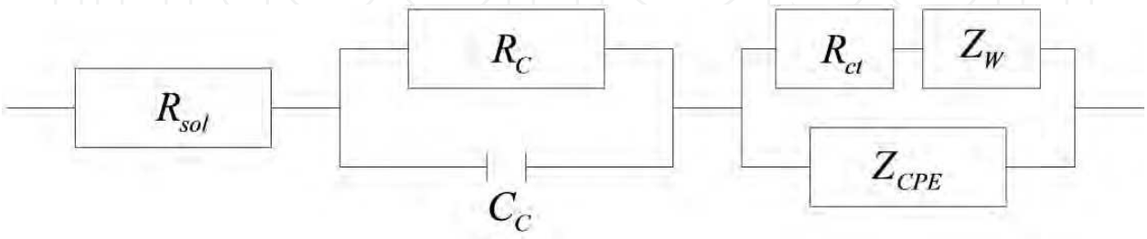

Fig. 9. Equivalent circuit for carbon steel in cement mortar

26℃	R_s Ω·cm²	R_c Ω·cm²	10^9C_c F·cm²	$10^{-3}R_{ct}$ Ω·cm²	10^3Y_{0w} Ω⁻¹·cm⁻²·S$^{1/2}$	10^4Y_{0dl} Ω⁻¹·cm⁻²·S^n	n
0.5%	191.6	342.6	9.604	3.998	1.777	1.074	0.7155
1.0%	132.8	316.5	6.254	2.340	1.489	1.162	0.7723
3.0%	123.2	247.8	80.80	2.606	1.692	1.374	0.9339
5.0%	109.6	219.3	25.54	0.6511	2.783	1.482	0.7936

Table 2. Fitting results of $R_s(R_cC_c)((R_{ct}Z_W)Z_{CPE})$ at 26℃

50℃	R_s Ω·cm²	R_c Ω·cm²	10^9C_c F·cm²	$10^{-3}R_{ct}$ Ω·cm²	10^3Y_{0w} Ω⁻¹·cm⁻²·S$^{1/2}$	10^4Y_{0dl} Ω⁻¹·cm⁻²·S^n	n
0.5%	127.66	289.4	3.897	1.349	4.942	1.900	0.7329
1.0%	100.2	257.3	46.74	0.2906	2.169	2.720	0.8054
3.0%	108.1	218.2	21.15	0.1172	0.994	3.596	0.7625
5.0%	93.18	195.0	2.005	0.1507	6.326	3.469	0.6060

Table 3. Fitting results of $R_s(R_cC_c)((R_{ct}Z_W)Z_{CPE})$ at 50℃

Either at 26℃ or 50℃, there are two semi-circles in the Nyquist plots. This indicates that there are two time constants. One is caused by the cement mortar around the carbon steel WE (at the high frequency region), the other is caused by the electric double layer (at the medium frequency region).According to Fig.6 a), with the increasing of the NaCl

concentration, the diameter of the semi-circle in Nyquist plot decreases gradually and the shape of the EIS spectra shows noticeable change. The phase angles in Fig.7 a) increase gradually as the concentration of NaCl solution increases from 0.5% to 5.0%. Also, R_{ct} values decrease from 3998Ω·cm² to 0.6511Ω·cm² and Y_{0dl} values increase from 10740Ω^{-1}·cm^{-2}·S^{n} to 14820Ω^{-1}·cm^{-2}·S^{n} at same time. Although there is a fluctuation of R_{ct} which is 2606Ω·cm² in value as the concentration of NaCl solution is 3.0%, the R_{ct} will decrease with the increasing of the NaCl solution concentration. During this process, the passive film has been destroyed by the chloride ion. The chloride ion which is from the environment penetrates into the mortar and accumulates in the steel/mortar interface. This can cause the initiation and propagation of pitting corrosion. The destroying process of the chloride ion is accelerated by increasing the concentration of NaCl solution. The results show that the high concentration of NaCl solution will accelerate the influence of diffusion effect.

Smearing phenomenon has appeared in the low frequency region. This indicates that the diffusion process is the controlling process. Warburg impedance Z_w in Eq. (8) is often used to describe the semi-infinite plane diffusion's characteristic of oxygen. The Warburg diffusion process results from the diffusion of oxygen through the mortar to the steel/mortar interface. During this period, the system is limited by the diffusion process of oxygen. The Y_{0w} shows a fluctuant tendency in Table 2 and Table 3, which indicates that the concentration of NaCl solution has no significant influence on the diffusion process of the oxygen. But as the temperature is increased to 50℃, the value of Y0w is greater than its value with the same concentration of NaCl solution at 26℃.So the diffusion process proceeds more easily with the increasing of the temperature.

3.3 EN Feature of the RC system

3.3.1 Wavelet backgrounds

The wavelet analysis is a relatively new way of signal processing. It can overcome the problems of traditional Fourier transform. The continuous wavelet transform was proposed by Grossman and Morlet in 1984 [35]. Daubechies [36] constructed families of compactly supported wavelets. Mallat introduced the multi-resolution signal decomposition (MRSD) algorithm [37]. Since then the research in this field has progressed rapidly. The detailed description about wavelet transform can be found in the correlative literatures [38-40]. A wavelet is an oscillatory、real or complex function of zero average and finite length. The wavelets approach consists essentially in representing the time record $x_n(t), n = 1,2,...,N$ by special functions. By scaling and translating the father wavelets φ and the mother wavelets ψ as equation (12) and equation (13), the special functions which is a linear combination of basis functions $\varphi_{j,k}$ and $\psi_{j,k}$ can be generated.

$$\varphi_{j,k}(t) = 2^{-j/2}\varphi\left(2^{-j}t - k\right) = 2^{-j/2}\varphi\left(\frac{t - 2^j k}{2^j}\right) \tag{12}$$

$$\psi_{j,k} = 2^{-j/2}\psi\left(2^{-j}t - k\right) = 2^{-j/2}\psi\left(\frac{t - 2^j k}{2^j}\right) \tag{13}$$

Where $k = 1,2,\cdots,N/2^J$; and $J = 1,2,\cdots J$; J is often a small natural number which depends mainly on N and the basis function.

The time signal $x(t)$ can be represented as follows:

$$x(t) \approx \sum_k s_{J,k}\varphi_{J,k}(t) + \sum_{j=1}^{J}\sum_k d_{j,k}\psi_{j,k}(t) \tag{14}$$

Where $s_{J,k}$ and $d_{j,k}$ are so-called wavelet coefficients.

Unlike conventional techniques, wavelet decomposition produces a family of hierarchically organized decompositions. At each level j, the j-level approximation $A_j(t)$, and a deviation signal called the j-level detail $D_j(t)$ can be calculated according to the following equations.

$$A_j(t) = \sum_k s_{J,k}\varphi_{J,k}(t) \tag{15}$$

The detail $D_j(t)$ is defined as,

$$D_j(t) = \sum_{k\in Z} d_{j,k}\psi_{j,k}(t), j,k \in Z \tag{16}$$

$$d_{j,k} = \int_{-\infty}^{+\infty} x(t)\psi_{j,k}(t)dt \tag{17}$$

Decomposed process of the signal by wavelet transform can be illustrated as Fig.10.

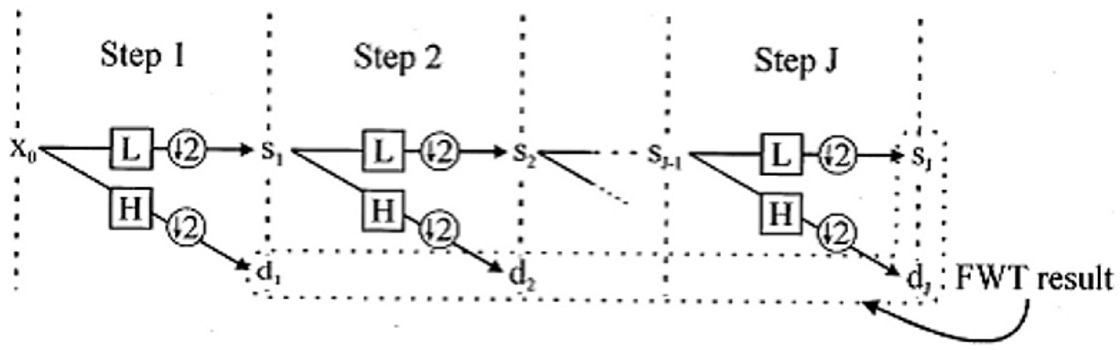

Fig. 10. General scheme of the FWT algorithm

The contribution of each crystal to the overall signal can be estimated by energy distribution plot (EDP), which is the plot of the relative energy accumulated by each crystal versus the crystal name. The term "crystal" is used because the wavelet coefficients in a crystal correspond to a set of translated wavelet functions arranged in a regular lattice. The energy E of the whole signal is calculated as follows:

$$E = \sum_{n=1}^{N} x_n^2, \quad n = 1,2,...,N \tag{18}$$

The relative energy corresponding to each crystal can be calculated as follows:

$$E_j^d = \frac{1}{E}\sum_{n=1}^{N/2^j} d_{j,n}^2,\ \ j = 1,2,...,J \tag{19}$$

$$E_j^s = \frac{1}{E}\sum_{n=1}^{N/2^j} s_{J,n}^2 \tag{20}$$

Because the Symlet wavelet is orthogonal, the following equation is satisfied:

$$E = E_J^s + \sum_{j=1}^{J} E_j^d \tag{21}$$

According to Eq. (19), (20) and (21), the EDP can be plotted[8].

3.3.2 Wavelet analysis of EN

The electrochemical potential noise (EPN) and electrochemical current noise (ECN) are listed in Fig.11 and Fig.12 respectively[8]. The NaCl solution is not injected at this time. From Fig.11 we can see there is a DC trend from -0.61315V to 0.61689V in the EPN data. The amplitude of the EPN in Fig.11 is very low (10^{-5}V degree).Fig.12 shows the ECN before NaCl solution is injected. The current amplitude is 10^{-7}A degree which almost remains unchanged in all the time-record. Also, there is a DC trend in the ECN data. The frequency of the signal in ECN and EPN is very high. From Fig.16 and Fig.12 we can see that the signals are caused by the measuring apparatus and the concrete-steel system. But the amplitude of EPN and ECN is very low and the accuracy is satisfied.

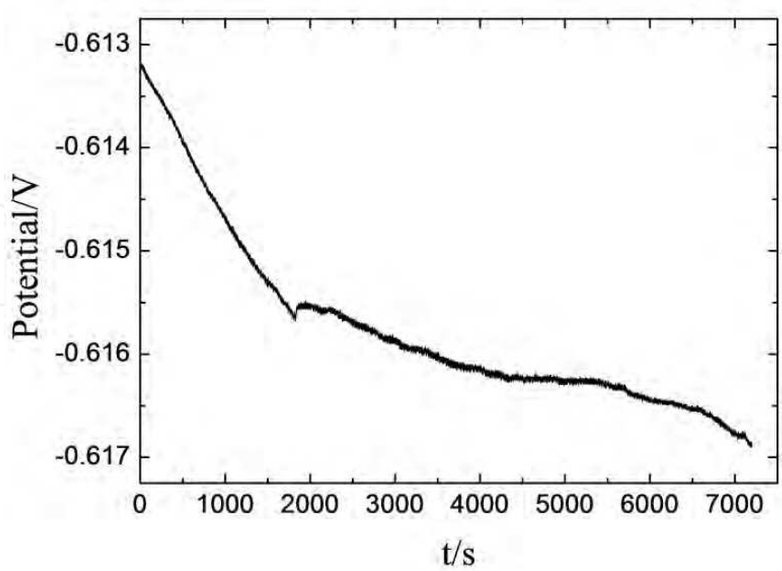

Fig. 11. EPN before NaCl solution injected

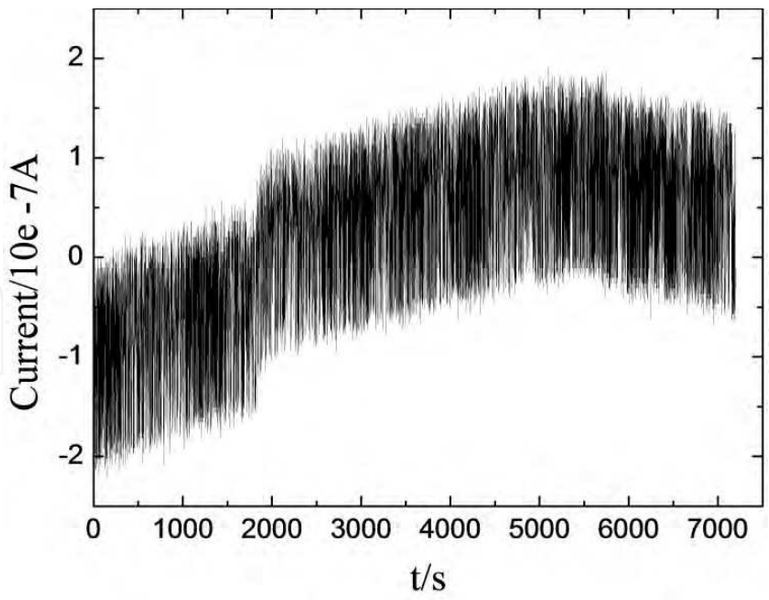

Fig. 12. ECN before NaCl solution injected

Fig.13 and Fig.14 show the EPN and ECN which are sampled after 3.0% NaCl solution is injected into the specimen respectively. The sampling frequency is 2Hz. Also, there is a DC trend in Fig.13 and Fig.14. The DC trend of EPN in Fig.13 is much greater than the DC trend of ECN in Fig.14. There is characteristic of pitting corrosion which is shown as EPN transients in Fig.13. The smaller Fig. in Fig.13 shows a characteristic transient which is chosen stochastically. From the smaller Fig. we can see that the amplitude of the EPN transient which changes from -0.534V to -0.538V is very large (The degree of EPN in Fig.11 is

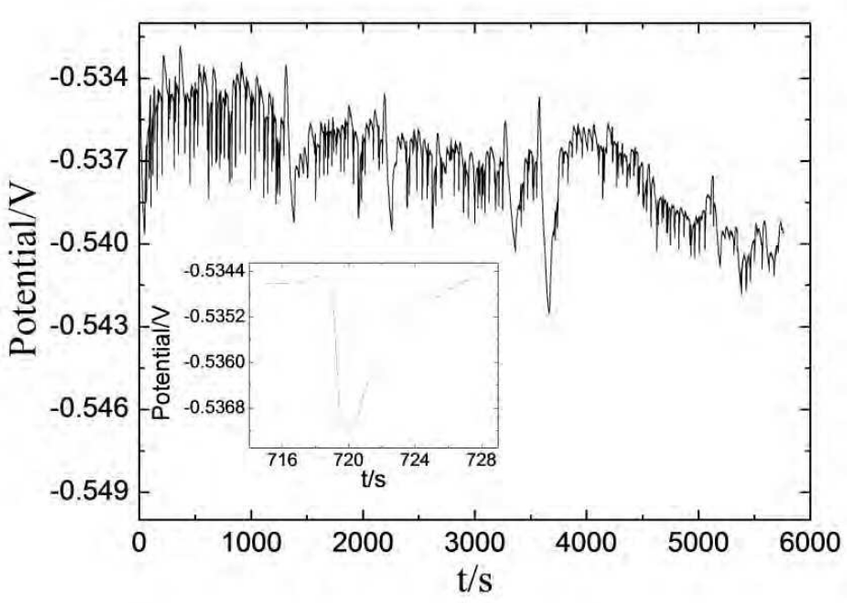

Fig. 13. EPN after 3.0% NaCl solution injected

only 10^{-5}V). The duration of the transient is several tens of seconds (It is 20 seconds in the smaller Fig.). The characteristic of the transient is that it decreases suddenly and recovers slowly. There is a much gentler DC trend in Fig.14. The amplitude of the ECN is 10^{-6}degree (It is 10^{-7}degree in Fig.12). The minus sign of the ECN means that the current is flows from identical CE to the WE. The smaller Fig. in Fig.14 shows the characteristic transient of the ECN. It increases sharply and recovers slowly. It must be kept in mind that here the current 'increases' is from plus sign to minus sign. Also its duration is several tens of seconds. According to D.Macdonald's PDM, the aggressive anion Cl^- is able to enhance the flux of cation vacancies through the barrier layer. Under favorable conditions (voltage, PH, [Cl^-]) vacancy condensation will occur at the metal/barrier layer interface and hence passivity breakdown will ensue. So, the fresh surface of the metal will generates EPN and ECN transients.

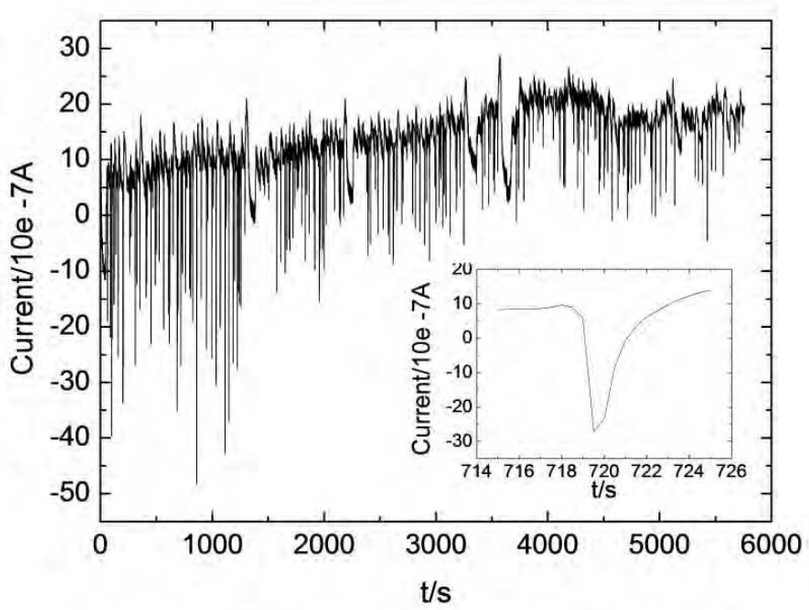

Fig. 14. ECN after 3.0% NaCl solution injected

Sym4 wavelet is used to decompose the EPN and ECN signal from j=1 scale to j=8 scale. The crystals from d_1 to d_8 are the details of the signal. a_8 is the approximation part of the signal. From the decomposed results we can see that the signal energy is stored in approximation crystal a_8 and detail crystals which are from d_1 to d_8.The approximation a_8 is the principal part of the DC trend. It contains most of the energy of the signal. In order to eliminate the DC trend influence, the energy of a_8 is not be considered in the calculation. In this way, we can remove the DC trend.

Fig.15 and Fig.16 show the EDP of EPN in Fig.11 and Fig.13, respectively[8]. According to Fig.15, the detail signal energy accumulates in crystal d_1 to d_4. They are the high frequency information of the signal in Fig.11. The energy in crystal d1 to d4 almost occupies 80% of the whole detail energy. But in Fig.16, most of the energy accumulates in the low frequency crystal, such as d_4, d_5, d_6 and d_7. According to Fig.13 and Fig.14, we can see that the low frequency parts in Fig.16 correspond to the transient of the pitting corrosion. The fact that the energy distribution changes from high frequency parts in Fig.15 to low frequency parts

in Fig.16 shows that the EPN transients emerge and become the dominant parts gradually. From Fig.17 we can see that most of the energy of the detail information in Fig.12 accumulates in crystal d_1, d_2, d_3 and d_8. There is a little difference between Fig.17 and Fig.15. In Fig.15 the energy in crystal d8 is very small(less than 0.025), but in Fig.17 the energy in crystal d_8 is large than 0.2. This can be caused by the frequency component in ECN. Although we have removed most of the DC trend in Fig.14 by eliminating the crystal a_8, the very low frequency which is very less will exist in crystal d_8.So we can see the higher energy ratio of crystal a_8 in Fig.17 and Fig.18. When 3% NaCl solution is injected into the specimen by high pressure pump, we can see that the energy in d_4、d_5、d_6 and d_7 becomes more significant. In Fig.17, the energy in crystal d_4、d_5、d_6 and d_7 is less than 0.2 of the whole detail information, but in Fig.18, it increases to no less than 0.6. This also means that the current transient becomes the main component in the ECN. The current transient is caused by the pitting corrosion, so the change of EDP can show the corrosion mechanism.

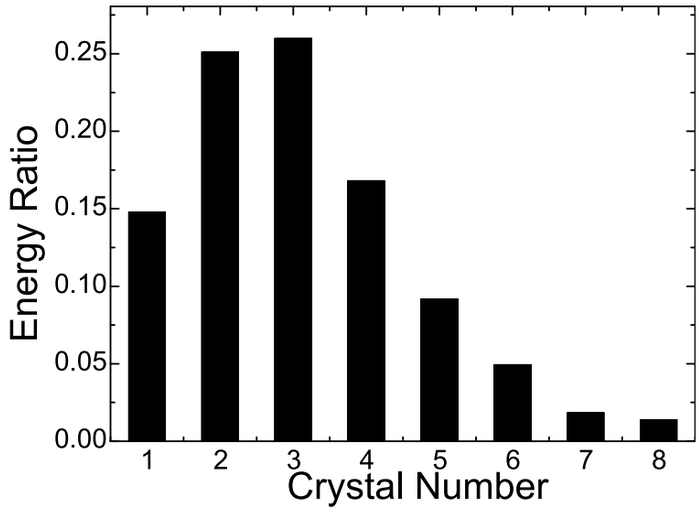

Fig. 15. EDP of EPN before NaCl solution injected

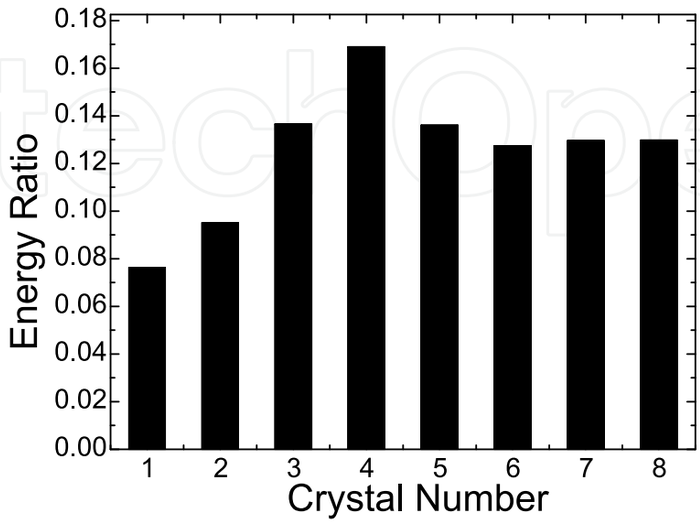

Fig. 16. EDP of EPN after NaCl solution injected

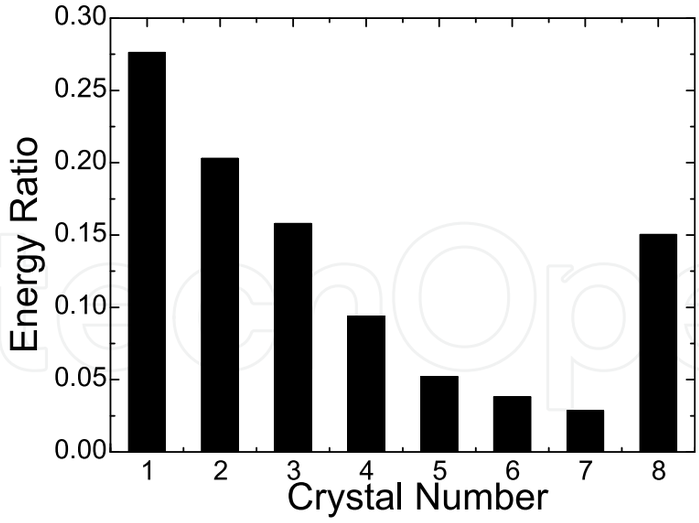

Fig. 17. EDP of ECN before NaCl solution injected

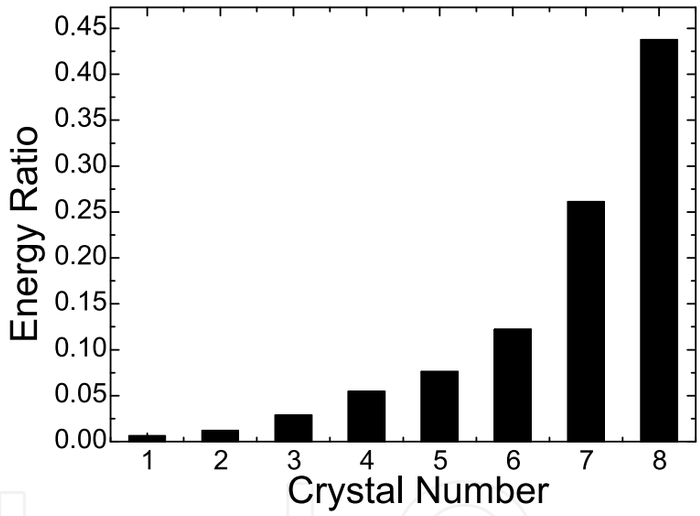

Fig. 18. EDP of ECN after NaCl solution injected

4. Corrosion sensors and networks

4.1 Solid-state reference electrode

Monitor and control the corrosion of reinforcing steel in concrete require reliable measurement of stable potentials. Therefore, embeddable reference electrodes(RE) is the key element in corrosion monitoring of concrete structures for long-term monitoring and potentiostatically controlled cathodic protection of reinforcement in concrete[41]. A practical RE have to obey the following conditions: it must be stable, invariant to chemical change in concrete, tolerant to climatic conditions and have the ability to pass small currents with a minimum of polarization and hysteresis effects, display long term performance, be cost effective and result from an environmentally safe manufacturing process [42]. Traditional liquid references, such as the standard hydrogen electrode (SHE), the saturated calomel

electrode (SCE) and the copper/copper sulfate reference electrode (CSE), etc., are conventionally used for the most laboratory experiments in most conditions due to its reliable performance. Unfortunately, the short service life and fragile structure determine these reference electrodes can not be used in the field. Recently, several embeddable REs, such as MnO_2 [43-47], Metal-Metal Oxide (MMO) [48, 49] and $NiFe_2O_4$ [50], have been prepared and attempted to apply in RC structures. European Federation of Corrosion (EFC) has also reviewed the electrochemistry and characteristics of embeddable reference electrodes for concrete, and reported the service status of the six kinds of embeddable REs which have been implanted in Gimsøystraumen Bridge (in Norway) few years ago[51]. It can be seen clearly from the foregoing that there is an utmost need to develop and evaluated the performance of reliable and maintenance-free REs for use in concrete [52, 53]. Compared with that of the other REs, the RE based on Ag/AgCl is stable, easily prepared and industrialized conveniently, and have been used in electrochemistry for a long period[54]. Although the RE based on Ag/AgCl can not be applied directly in reinforcing concrete structures currently, its performance can be improved greatly by the elaborate design of the materials and the structure. PTFE, Al_2O_3 and AgCl powder are applied as the carrier material and enhanced substance to improve the behavior of the RE, respectively.

A novel Ag/AgCl based solid-state RE has been prepared and characterized to provide the key element for the potential control of the corrosion monitoring sensors(see Fig.19)[55]. Long-term stability, temperature response, anti-polarizability and anti-disturbance of ions have been investigated. The results indicate that the balance potential of the reference electrode is 3.64 mv±1mv (vs.SCE) at 25℃. The temperature response coefficient of the RE is -0.51 mv/℃±0.03mv/℃ in [10℃, 70℃]. Also, the anti-polarizability of the solid-state RE meets the requirements of the electrochemical measurement in the field. Additionally, the reference electrode is insensitive to the concrete admixtures which include Na_2SO_4, NaCl, $NaNO_3$ and $NaNO_2$.

Fig. 19. Solid-state reference electrode

4.2 Wired corrosion monitoring sensors

The five-electrode corrosion sensors have been applied to monitor the corrosion state of the reinforcing steel in the beams[55]. There are four kinds of elements which include one reference electrode(RE), one counter electrode(CE) and three identical working electrodes(WEs) in the corrosion sensor. Considering the field applicability, a home-made all solid-state reference electrode (ASSRE) has been used to setup the five-electrode corrosion sensor. The materials of the counter electrode and working electrodes are the graphite rod and the Q235 carbon steel, respectively. One of the three working electrodes, CE and ASSRE are integrated as classical three-electrode system to execute the galvanostatic step measurement. The other two identical working electrodes and ASSRE are applied to obtain the EN data. The sampling frequency of EN is 2Hz. Fig.20 shows the photograph of the corrosion sensors.

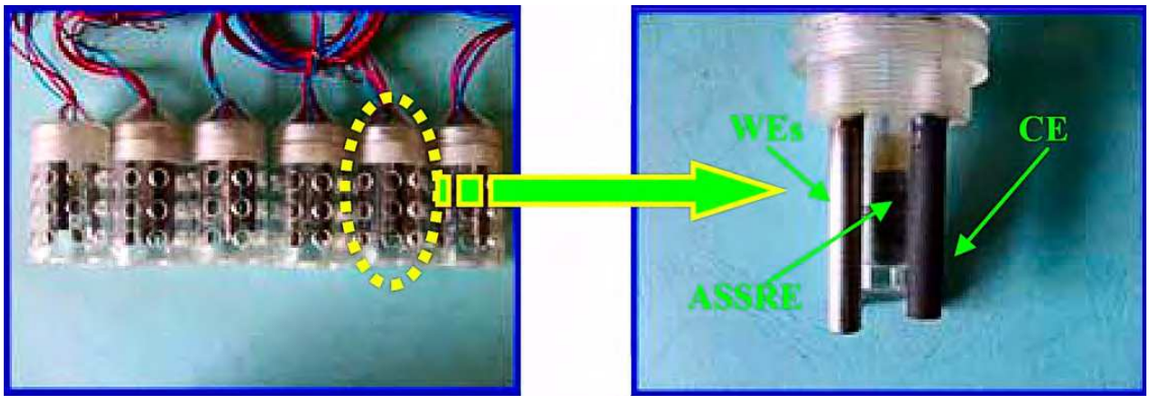

Fig. 20. Five-electrode corrosion sensors

The current confining sensor has been developed for RC structures[56]. Fig 21 illustrates the geometric configuration of the sensor. The red ring is the counter electrode(CE). The other two yellow rings beside the CE are the current confining rings. Two all solid-state reference electrodes (ASSREs) are applied to sense the potential of the concrete between the counter

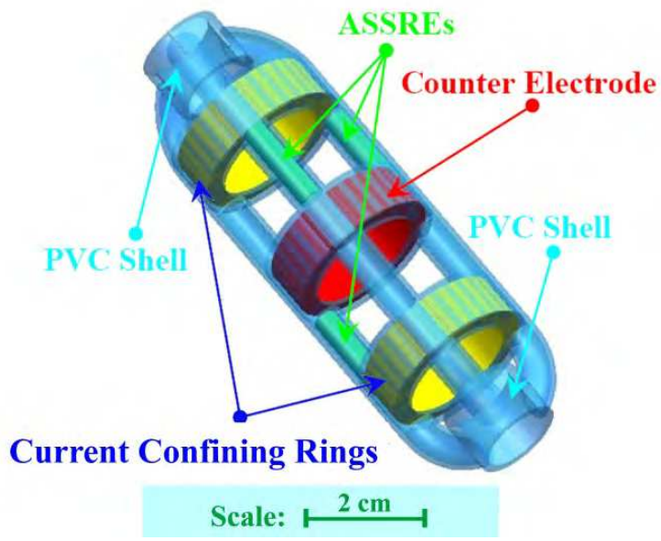

Fig. 21. Solid state and current confining corrosion sensor

electrode and the current confining rings. The third ASSRE is used as the normal reference electrode(RE) of the traditional three-electrode system in electrochemical techniques to measure the potential of the working electrode(WE). Here, WE is the reinforcing steel in RC structures. The potential of the counter electrode and the current confining rings is controlled by the embedded microcircuit of the data acquisition and processing system. The geometric configuration of the sensor is optimized by the Finite Element Method (FEM). the electric fluxline can be effectively confined in a fixed area on the surface of the steel bar between the CE and the other two rings. Therefore, the corrosion rate of the reinforcing steel in RC structures can be measured accurately by the optimized corrosion sensor.

4.3 Self-powered wireless corrosion monitoring sensors & networks

For an airtight civil engineering structure(for example, concrete beam), while a wire collection system is used for monitoring corrosion, the wire put inside concrete beam needs to prolong outside concrete beam to send the corrosion sensor's information, which will accelerate the corrosion process because the wire's laying possibly makes reinforcing steel inside the beam contact with air. Wireless sensor networks with wide application especially in structural health monitoring[57-60], matured in recent years represent an innovative solution to current corrosion monitoring systems, due to their low-cost, small size, low-power and wireless communication capability.

The most interesting and fascinating fact is that the corrosion process is an energy release process. This vital energy provides the possibilities to realize in-situ, real-time and on-line corrosion monitoring of RC structures by wireless energy-harvesting sensors and networks. We investigate deeply the generation of corrosion energy in RC structure and its availability as a power source. Powered by the energy harvested from corrosion environment, a new smart sensor platform is then designed to detect the corrosion status and report the samples via wireless links to the end user. Developing energy harvesting sensors is of critical importance for in-situ, real-time and on-line corrosion monitoring of RC structures because of its intrinsic capability of providing unbounded lifetime. This represents a tremendous step towards realization of practical corrosion monitoring.

For a wireless sensor network, energy is usually provided from either solar power[61], structure vibration[62], chemical batteries, or lithium batteries. The wireless corrosion monitoring sensors need to be put inside concrete beam in an airtight way, which require that wireless sensor can work for a long time without outside energy supply as corrosion is a slow process(about tens years). Thus it is necessary to solve the problem of energy supply for the sake of monitoring corrosion with wireless sensor networks.

In the proposed self-powered wireless corrosion monitoring sensor network system shown in Fig.22[63], we use the electrochemical noise produced by corrosion not only as sensing signal but also as energy source for wireless sensor, the process of monitoring corrosion is the following: unit of gathering energy collect electrochemical noise, while energy reach the working requirement of wireless sensor, the other units of wireless corrosion sensor are in activation. Then micro-processing unit gathers and process the sensor signal--electrochemical noise, the sensor signal processed is little in volume for wireless transmission because the energy needed by wireless transceiver unit is much more largely than the one of micro-processing unit. All the above units are put together inside airtight concrete structure to integrate into a self-powered wireless corrosion monitoring sensor, lots of such sensors forming self-organizing networks send their signal information to wireless base station. Wireless base station may receive the information and control the sensors,

remote users can visited wireless base station to know the sensors' status and corrosion information of monitored objective. The designed self-powered wireless corrosion sensor is exhibited in Fig.23[64].

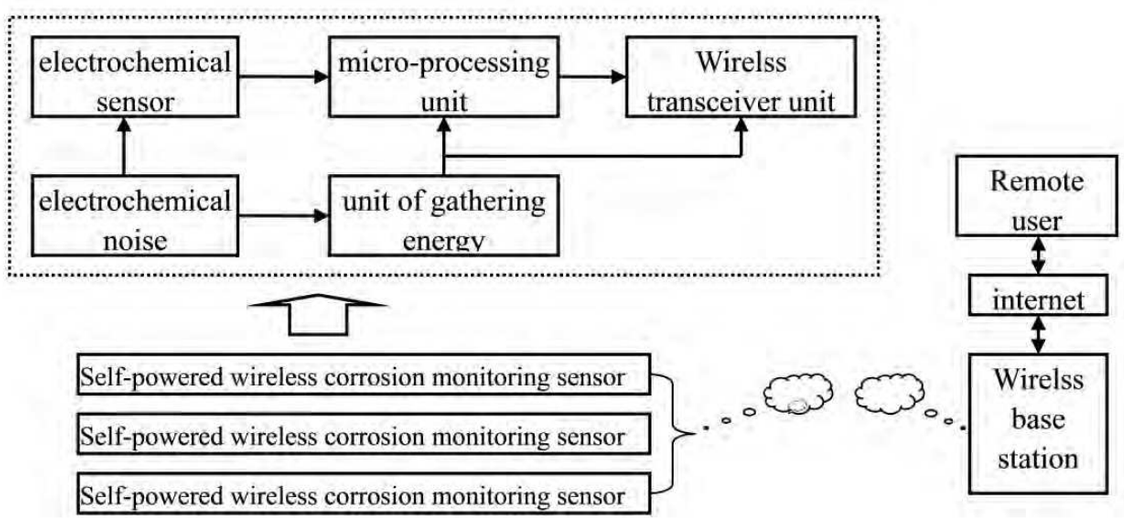

Fig. 22. Self-powered wireless corrosion monitoring networks

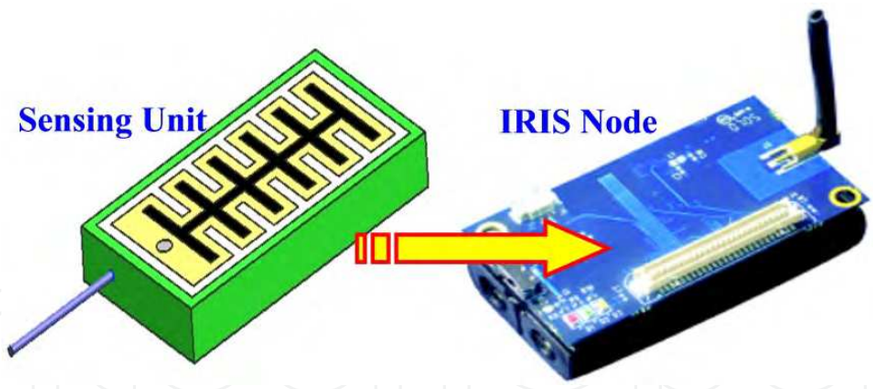

Fig. 23. Self-powered wireless corrosion monitoring sensor

5. Application of the corrosion monitoring system in civil engineering

5.1 Corrosion monitoring of the RC beams

The corrosion sensors presented in the previous sections have been applied to monitor the corrosion status of the RC beams (see Fig.24). The electrochemical measuring techniques which are seemed as the software for corrosion monitoring based on galvonastatic step excitation and electrochemical noise have been developed to extract the characteristics of general corrosion and pitting corrosion, respectively[65].

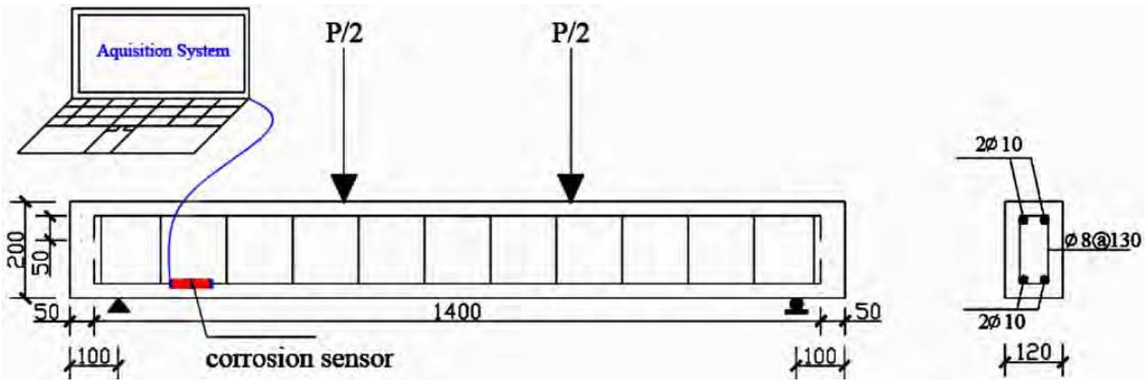

Fig. 24. Distributed bars, sectional dimension and the position of the corrosion sensors.

5.1.1 Half-cell potential map

Fig.25 shows the half-cell potential results of the beams. The half-cell potential of all the bars are higher than -200mv (Vs. CSE) before corrosion. According to ASTM C876-91, the corrosion probability of the steel bar is no more than 5% and the deterioration effect of the corrosion can be neglected. However, the potential shifts towards negative severely after corrosion. The potential in most measuring points is less than -400mv (Vs. CSE) after corrosion. Some of the measuring results are even less than -1000mv. This can be explained by the non-homogeneous corrosion of the steel bar. Actually, there are many defects in the

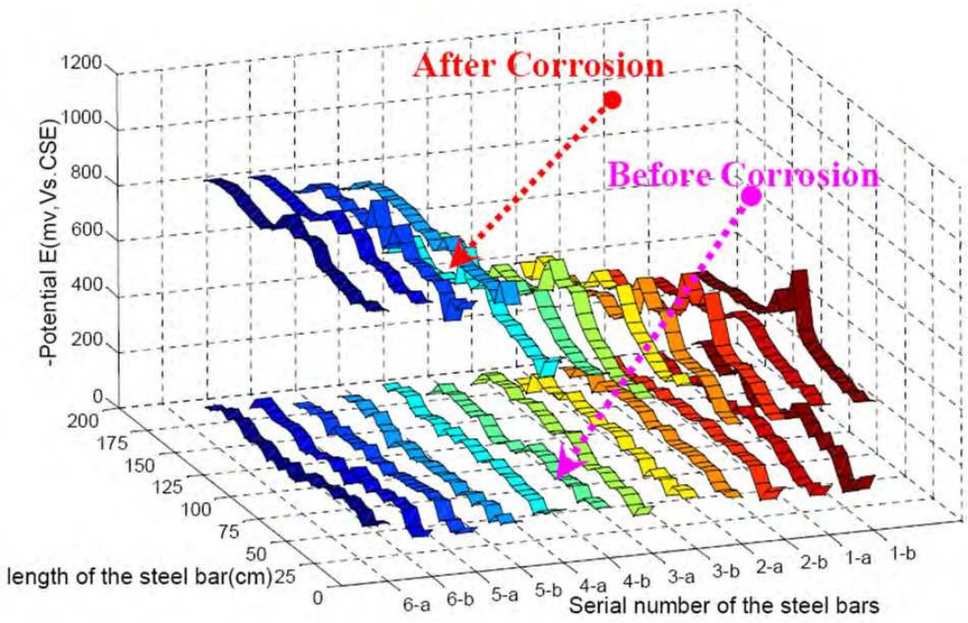

Fig. 25. Half-cell potential of the RC beams

concrete. The corrosion of the steel bar in these defects is much more severely than that of the other sections. The corrosion probability of the beam is more than 95% after corrosion. Comparing the results of the beam1# to that of the beam 6#, the potential becomes much more negative when the corrosion is more severe. But it must be mentioned that the corrosion products and the water saturated degree of the concrete can influence the accuracy of the potential results. There are minimums in each bar's half-cell potential. Such as the steel bar 1-b, the minimum of the potential is -725.2mv (Vs.CSE) in the middle of the beam. This phenomenon is due to the local corrosion of the steel bar. The reddish-brow corrosion product perspires from the concrete crevice during the accelerating process.

5.1.2 Transient potential response

Five pieces of RC beams which is from the beam 2# to the beam 6# have been tested in the experiments. Considering the length of the paper, we only show the typical results of the beam 2# in Fig.26. According to the plots of the potential response, we can see clearly that the potential response can not reach the steady state even as the current has been applied for 1000s. This is due to the diffusion process of the oxygen. The accelerating corrosion process has consumed too much oxygen in the pore of the concrete to meet the requirements of the cathode reaction. Thus, the electrochemical process is controlled by the diffusion process. The method which has been derived in the previous section is used to analyze the data of the potential response. The fitting results are listed in Table 4. According to the results, the resistance of the concrete decreases gradually. The mean value of the concrete resistance decreases from 546.89Ω·cm² to 275.79Ω·cm² as the accelerating degree increases gradually from the beam 2# to the beam 6#. There are much more Cl^- concentrated in the pore of the concrete in the beam 6# than that of the beam 2#. The corrosion products of the steel bar have precipitated in the pore. Therefore, these two aspects can lead to the decrease of concrete resistance.

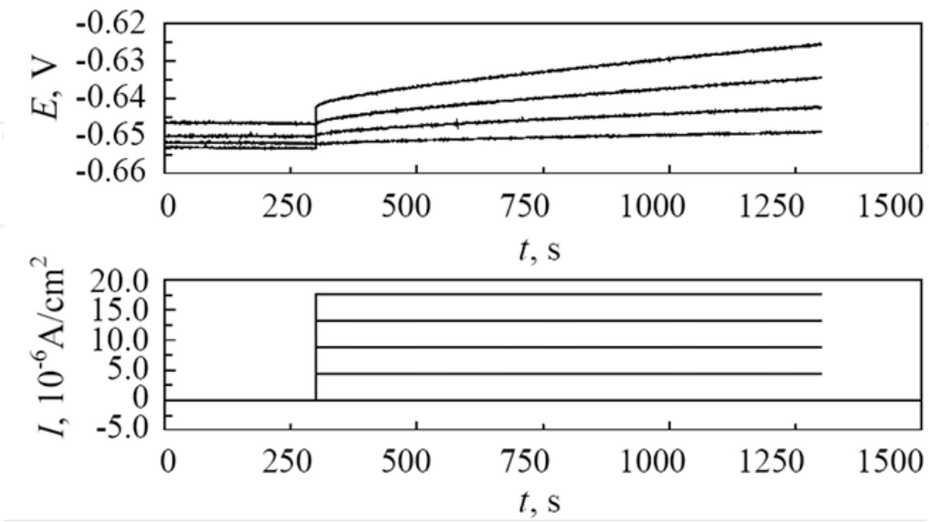

Fig. 26. The potential response of the beam 2#

Parameters		R_c $\Omega \cdot cm^2$	R_p $\Omega \cdot cm^2$	C_{NI} $10^{-4}F/cm^2$	τ_c s	K	σ $\Omega \cdot cm^2 \cdot s^{-1/2}$
2#	5uA/cm²	537.64	422.84	3.8355	0.16218	0.81683	38.457
	10 uA/cm²	551.48	415.65	3.1425	0.13062	0.80325	32.309
	15uA/cm²	545.57	437.50	3.2663	0.14290	0.84104	30.391
	20 uA/cm²	552.86	444.21	3.3560	0.14908	0.80152	30.971
3#	5uA/cm²	285.12	404.26	6.1530	0.24874	0.74654	13.694
	10 uA/cm²	251.19	415.95	3.9900	0.16596	0.76499	12.344
	15uA/cm²	271.53	416.49	4.2485	0.17695	0.70294	12.251
	20 uA/cm²	297.32	440.24	6.2499	0.27515	0.55664	12.353
4#	5uA/cm²	419.49	376.16	4.0576	0.15263	0.74447	15.297
	10 uA/cm²	435.69	391.05	3.4091	0.13331	0.90131	17.379
	15uA/cm²	448.40	387.00	3.1530	0.12202	0.88753	18.756
	20 uA/cm²	444.86	397.21	3.3036	0.13122	0.87004	19.112
5#	5uA/cm²	323.99	422.92	4.7930	0.20271	0.95230	17.243
	10 uA/cm²	310.63	432.48	4.1350	0.17883	0.84943	18.119
	15uA/cm²	305.13	428.50	4.1777	0.17901	1.00000	18.314
	20 uA/cm²	307.18	431.41	4.5445	0.19605	0.84993	18.934
6#	5uA/cm²	267.63	350.31	7.1249	0.24959	0.74114	19.628
	10 uA/cm²	278.01	373.64	6.3498	0.23725	0.74691	22.026
	15uA/cm²	280.34	372.49	5.9271	0.22078	0.90379	24.376
	20 uA/cm²	277.16	373.59	6.3188	0.23606	0.84188	25.230

Table 4. Fitting results of the response to galvanostatic step excitation

Also, the polarization resistance decreases gradually from the beam 2# to the beam 6#. This means that the content of the chloride ion can influence the corrosion rate of the steel bar. Much more Cl^- can destroy the passivity film much more severely. The magnitude of the non-ideal capacity C_{NI} is 10^{-4} F/cm2. The magnitude of the time constant $\tau_c=C_{NI}R_P$ is 10^{-1} second. R_P and C_{NI} are the essential characteristics related to the electrochemical process and the double layer. They do not depend on the WE's area, the resistance of the concrete and other factors. Therefore, τ_c which has many advantages than that of Half-cell potential can be used to determine qualitatively the corrosion status of the structure. According to the results of τ_c, the steel bar in the concrete has been corroded severely. Most of the K values are less than 1.This means that the CPE presents in the EC. The magnitude of σ and σ/R_p are $10\Omega \cdot cm^2 \cdot s^{-1/2}$ and more than 10^{-2}, respectively. These results show that the diffusion process controls the electrochemical reactions.

5.1.3 Electrochemical noise results

The EN of the beams from 1# to 6# has been obtained before and after accelerating corrosion. Also, we only show the results of the beam 2# here in Fig.27 and Fig.28, respectively. According to Fig.27 a) and Fig.28 a), we can see there is an obvious trend in the electrochemical potential noise (EPN) before and after corrosion. The electrochemical current noise (ECN) is much more stationary than that of the EPN in Fig.27 and Fig.28. The

magnitudes of the EPN and ECN before corrosion are 2mv and 10^{-7}A, respectively. The high frequency components (≤2 Hz) exhibit as white noise in the EN before corrosion. The distribution of the EN takes on the band form before corrosion. However, a large number of transients present in the EN record after corrosion. Compared to the EN before corrosion, the magnitude of the transients is very enormous after corrosion. The magnitudes of EPN and ECN are 10mv and 10^{-6}A, respectively. The transient increases sharply and recovers slowly, and its duration is tens of seconds. According to D.Macdonald's PDM, the aggressive anion Cl^- is able to enhance the flux of cation vacancies through the barrier layer. Under favorable conditions (voltage, PH, [Cl^-]), vacancy condensation will occur at the metal/barrier layer interface, and hence passivity breakdown will is confirmed. So, the fresh surface of the metal will generate EPN and ECN transients.

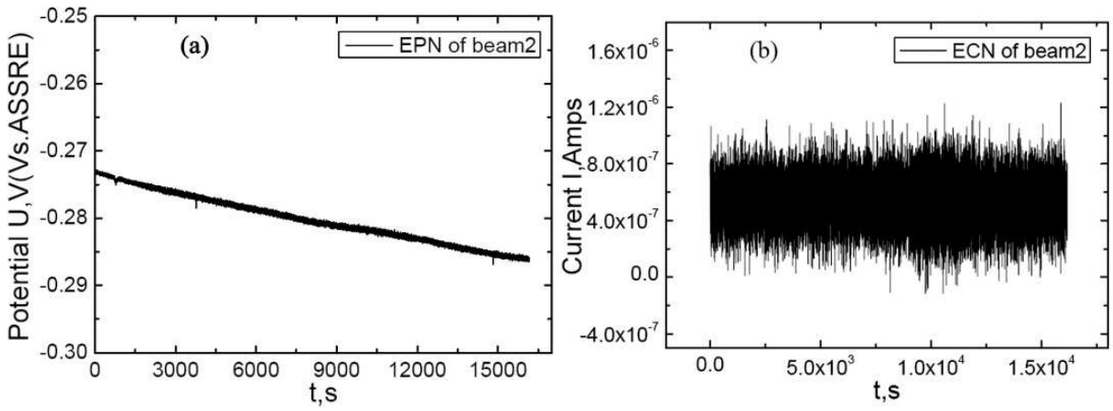

Fig. 27. EN of the beam 2# before corrosion. (a) Electrochemical potential noise. (b) Electrochemical current noise.

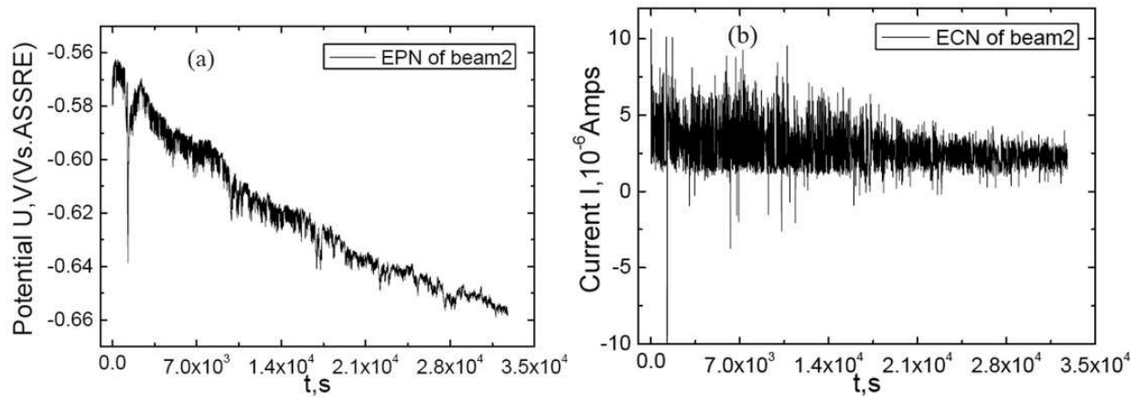

Fig. 28. EN of the beam 2# after corrosion. (a) Electrochemical potential noise. (b) Electrochemical current noise.

Sym4 wavelet has been applied to analyze the EN and the depth of the decomposing scale is 8 levels. The energy distribution plots of the EN before and after corrosion have been shown in Fig.29 and Fig.30, respectively. There are 9 parts of the signal after decomposition of the EN. The approximation of the EN which includes the trend of the EN is the lowest frequency part (≤0.004Hz). So, the signal of this part has been removed as the trend of the signal. The

energy distribution plots in Fig.29 and Fig.30 are the Energy ratio Vs. Crystal number which is from 1 to 8. According to Fig.29a), the energy of the EPN is concentrated on the crystal 1, 2 and 3 before corrosion. The frequency of these parts which is between 1Hz and 2-3Hz is much higher than that of other parts. It is much more obvious in Fig.29 b) that the energy is concentrated greatly on the crystals from 1 to 3. The energy of crystal 1 to 3 is no less than 70 percent of the signal in Fig.29 b). The signal in this much higher frequency range can be caused by the white noise of the system and the general corrosion of the steel-concrete system.

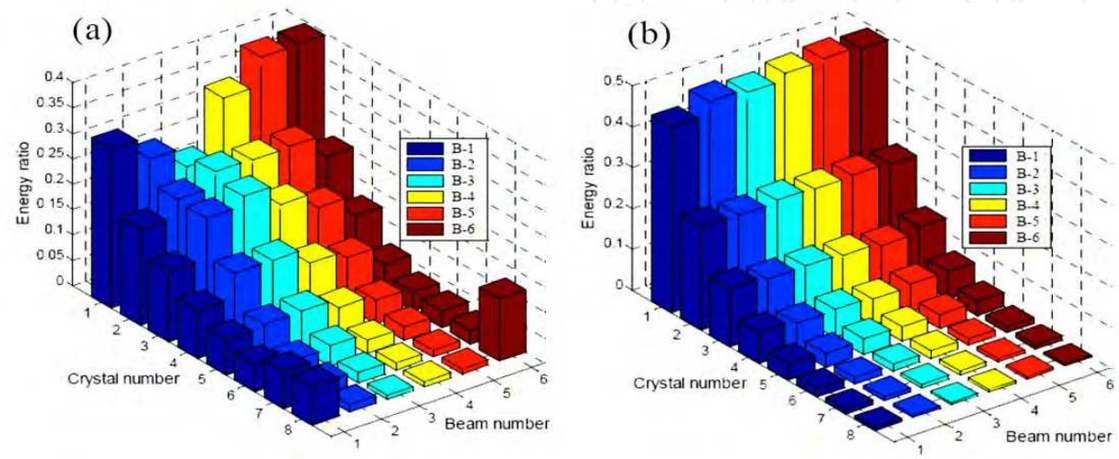

Fig. 29. Energy distribution plot of the EN before corrosion. (a) Electrochemical potential noise. (b) Electrochemical current noise. The histograms whose colors are from dark blue to dark red are the energy distribution plots of the beams which are from the beam1# to the beam 6#. The crystals which are from No.1 to No.8 are the energy concentrated on the different scales. The frequency range of the crystals which are from No.1 to No.8 decrease gradually. So the EN on No.1 level is the most detail part of the EN signal, but the EN on No.8 is much coarser than that of No.1.

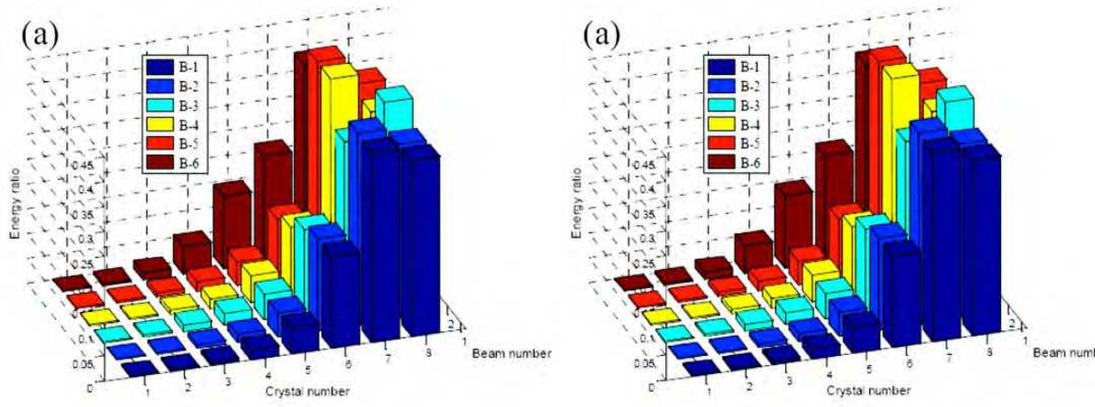

Fig. 30. Energy distribution plot of the EN after corrosion. (a) Electrochemical potential noise. (b) Electrochemical current noise. The means of the histograms in the Figures are same as that of Fig.29.

Compared with the results before corrosion in Fig.29, the energy distribution plot changes greatly after corrosion in Fig.30. The sum of the energy of the EPN on crystal 5, 6, 7 and 8 is

no less than 80 percent of the overall signal's energy which the approximation has been removed. The frequency of the crystals from 5 to 8 is no more than 2-5 Hz. The condition of ECN in Fig.12 b) is similar with that of the EPN in Fig.12 a). The energy on crystal 5, 6, 7 and 8 is more than 70 percent of the signal. The obvious difference of the EDP before and after corrosion is due to the different components in the EN. There are a large number of transients in the EN after corrosion. The transient is generated by the breakdown and recovery of the passivity film during the pitting corrosion process. The attenuation life of the transient is from tens of seconds to a few hundred seconds. Much more energy is concentrated on the crystals which are from No.5 to No.8. The change of the EDP indicates the change of the corrosion type. According to the change of the energy distribution on the different crystal, the pitting corrosion is verified. The energy which is distributed on the crystal 5, 6,7and 8 is the intrinsic characteristics of pitting corrosion of the steel bar in concrete. The EDP of the EN can be applied as the benchmark to identify qualitatively the presence of the pitting corrosion.

5.2 Corrosion monitoring of the bridge pier

The corrosion monitoring techniques and sensors presented in the previous sections have been integrated as corrosion monitoring system in Fig.31, and the system has been applied in the corrosion monitoring of the bridge pier (see Fig.32). The location of the corrosion sensors have been optimized according to the hot spot of the force and the deterioration caused by the ambience. The system has serviced for 1.5 year, and no corrosion sites have been founded till now.

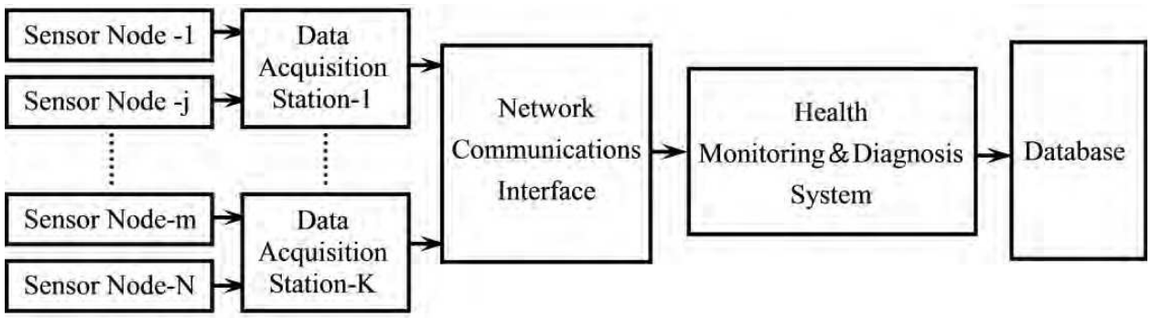

Fig. 31. Corrosion Monitoring System

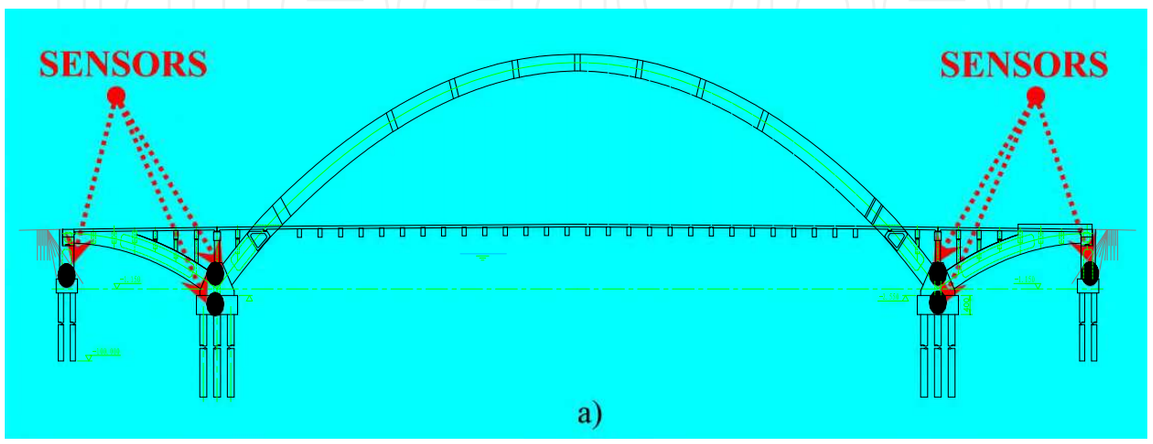

Fig. 32. Corrosion monitoring of the bridge pier. Scheme of the sensors' location a), Bird's eye view of the pier b) , and the sensor installation c)

6. Conclusions and prospects

With the development of global warming and further deterioration of the environment, the conditions of RC structures now becomes more atrocious than that of before. Reinforcement corrosion is the main cause of damage and early failure of reinforced concrete structures worldwide with subsequent enormous costs for maintenance, restoration and replacement. Corrosion monitoring will be very helpful for the safety assessment and service life prediction of RC structure. Although several kinds of corrosion monitoring sensors and

systems have been applied in petroleum industry, chemical industry and industrial factory buildings, there are many factors which handicap the development of corrosion monitoring in civil engineering structures. In the past few years, The Government of China has provided special found to do the research in the field of corrosion monitoring in concrete. The project includes four parts of work which are Research of Corrosion Monitoring Method, Development of Corrosion Sensor Platform, System Integration Technique and Safety Assessment & Life Prediction of Structure. The electrochemical essence of the corrosion process determinates that the corrosion monitoring sensor based on the electrochemical theory can be used effectively to realize the object directly. This provide the chance and challenge simultaneously to the researchers in the field of electrochemistry, material, computer, electronics, signal processing, mechanics, etc. A series of originality innovations should be developed in future.

The realization of the wired and self-powered wireless corrosion monitoring sensors and networks can be considered as a milestone in the field of SHM. Besides it can be used in civil engineering, the advantages of power harvesting, wireless, long-life and advanced EN technique, etc, determine the system can be applied widely in most formidable conditions, such as nuclear industry, petrochemical engineering and many other corrosion monitoring needed conditions.

7. Acknowledgment

This research is supported by grants from NSFC (Project No.: 51008098 and 50538020), National Science Fund for Distinguished Young Scholars (Project No.:50925829), Research Innovation Found of HIT (Project No.: HIT.NSRIF.2009 LPQQ57500095) and SZDCCE 10-09. Also, the financial support from Jilin Provincial Communications Department through the transport projects (Project No.: 2010-1-7) is grateful acknowledged.

8. References

[1] Sidney Mindess; J.Francis Young; David Darwin. (2002). *Concrete*. Prentice-Hall Inc., Canada

[2] D.Macdonald; Brian M.Marx. Development of Advanced Electrochemical Emission Spectroscopy for Monitoring Corrosion in Simulated DOE Liquid Waste. (2004). *Annual report of the project DE-FG07-97ER62515*

[3] V.Feliu; J.A.Gonzalez; C.Andrade. (1998). Equivalent Circuit for Modelling the Steel-Concrete Interface.I.Experimental Evidence and Theoretical Predictions. *Corros. Sci*., Vol. 39, pp. 864-882

[4] V.Feliu; J.A.Gonzalez; C.Andrade. (1998) Equivalent Circuit for Modelling the Steel-Concrete Interface. II. Complications in Applying the Stern-Geary Equation to Corrosion Rate Determinations. *Corros. Sci*., Vol. 40, pp. 995-1006

[5] Z.Sun; F.Mansfeld. (1999). Localization Index Obtained from Electrochemical Noise Analysis. *Corrosion*, Vol. 55, Issue 10, pp. 915-918

[6] Y.Y.Shi; Z.Zhang; J.Q.Zhang. (2008). Dimensional Analysis Applied to Pitting Corrosion Measurements. *Electrochimica Acta*., Vol. 53, pp. 2688-2698

[7] X.F. Liu; H.G. Wang; H.C. Gu. (2006). Fractal Characteristic Analysis of Electrochemical Noise with Wavelet Transform. *Corros. Sci*., Vol. 48, pp. 1337-1367

[8] Guofu Qiao, Jinping Ou. (2007). Corrosion Monitoring of Reinforcing Steel in Cement Mortar by EIS and ENA. *Electrochimica Acta*., Vol. 52, pp. 8008-8019
[9] S. Turgoose; R.A. Cottis. (1991). The Impedance Response of Film Covered Metals, *Conference Proceedings: Electrochemical Impedance Analysis and Interpretation*, San Diego, CA
[10] Li, T.C. Tan and J.Y. Lee. (1996). *Corros. Sci*., Vol. 38, pp. 1935-1939
[11] D.D. Macdonald; M.C.H. McKubre. (1981). Electrochemical Impedance Techniques in Corrosion Science. *Electrochemical Corrosion Testing*, *ASTM STP 727*, pp. 110
[12] D.D.Macdonald. (2006). Reflections on the History of Electrochemical Impedance Spectroscopy. *Electrochimica Acta*, Vol. 51, pp. 1376–1388.
[13] Y. Chen; W.P. Jepson. (1999). EIS Measurement for Corrosion Monitoring under Multiphase-flow Conditions. *Electrochimica Acta*, Vol. 44, pp. 4453-4464
[14] Schiessl P. (1988). *Corrosion of Steel in Concrete*. RILEM Technical Committee 60-CSC. New York: Chapman & Hall
[15] A. Aballe; M. Bethencourt; F.J. Botana; M. Marcos, J.M. Sanchez-Amaya. (2004). *Corros. Sci*., Vol. 46, pp. 1909
[16] A. Nagiub; F. Mansfeld. (2001). *Corros. Sci*., Vol. 43, pp. 2147
[17] R.J.K. Wood; J.A. Wharton; A.J. Speyer; K.S. Tan. (2002). *Tribol. Int.*, Vol. 35, pp. 631
[18] F. Mansfeld; L.T. Han; C.C. Lee; C. Chen; G. Zhang; H. Xiao. (1997). *Corros. Sci.*, pp. 255
[19] J.G. Yu; J.L. Luo; P.R. Norton. (2002). *Electrochim. Acta.*, Vol. 47, pp. 4019
[20] F. Mansfeld; Z. Sun; C.H. Hsu. (2001). *Electrochim. Acta*., Vol. 46, pp. 3651
[21] A. Nagiub; F. Mansfeld. (2002). *Electrochim. Acta.*, Vol. 47, pp. 2319
[22] A. Aballe; M. Bethencourt; F.J. Botana; M. Marcos. (1999). *Electrochim. Acta*., Vol. 44, pp. 4805
[23] R.J.K. Wood; J.A. Wharton; A.J. Speyer; K.S. Tan. (2002). *Tribol. Int.*, Vol. 35, pp. 631
[24] R.A. Cottis. (2001). *Corrosion*, Vol. 57, pp. 265
[25] J.F. Chen; W.F. Bogaerts. (1995). *Corros. Sci*., vol. 37, pp. 1839
[26] Y.F. Cheng; J.L. Luo; M. Wilmott. (2000), *Electrochim. Acta*., Vol. 45, pp. 1763.
[27] U. Bertocci; J. Frydman; C.Gabriclli; F.Huet; M.Keddam. (1998). *Electrochem. Soc*., Vol. 145, pp. 2780
[28] A. Aballe; M. Bethencourt; F.J. Botana; M. Marcos. (1999). *Electrochim. Acta*., Vol. 44, pp. 4805
[29] A. Aballe; M. Bethencourt; F.J. Botana; M. Marcos. (1999). *Electrochem. Commun*., Vol. 1, pp. 266
[30] F.H. Cao; Z. Zhang; J.X. Su; Y.Y. Shi; J.Q. Zhang. (2006). *Electrochim. Acta*, Vol. 51, pp. 1359
[31] C. Cai; Z. Zhang; F.H. Cao; Z.N. Gao; J.Q. Zhang; C.N. Cao. (2005). J. *Electroanal.Chem*., Vol. 578, pp. 143
[32] L. Mariaca; A. Bautista; P. Rodriguez; J.A. Gonzalez. (1997). *Mater. Struct.*, Vol. 30, pp. 613
[33] A. Legat; M. Leban; Z. Bajt. (2004). *Electrochim. Acta*, Vol. 49, pp. 2741
[34] R.G. Hu; C.J. Lin; B. Zhao; R.G. Du. (2005). *Proceedings of 16th International Corrosion Congress*, Paper 258, Beijing
[35] A. Grossman; J. Morlet. (1984). *SIAM J. Math*, Vo. 15, pp. 723
[36] I. Daubechies. (1988). *Commun. Pure Appl. Math*, Vol. 41, pp. 909
[37] S. Mallat. (1989). *IEEE Trans. PAMI*, Vol. 11, pp. 674
[38] I. Daubechies. (1992). *Ten Lectures on Wavelets*, SIAM Press, Philadelphia, USA

[39] G. Strang; T. Nguyen. (1996). *Wavelets and Filter Banks*, Wellesley–Cambridge Press, Wellesley, MA

[40] S. Mallat. (1998). *A Wavelet Tour of Signal Processing*, Academic Press, Oval Road, London

[41] Frank J. Ansuini; James R. Dimond. (2001). Long-term Field Tests of Reference Electrodes for Concrete- Ten Year Results. *Corrosion*, Paper No. 01296, pp. 1-13

[42] Leigh Ann Pawlick; Glenn E. Stoner; Gerardo G. Clemena. (1998). Development of an Embeddable Reference Electrode for Reinforced Concrete Structures. *Final Contract Research Sponsored by Virginia Transportation Research Council* (*A Cooperative Organization Sponsored Jointly by the Virginia Department of Transportation and the University of Virginia*), No. VTRC 99-CR1, pp.1-93

[43] Arup, H.; Sørensen, B. (1992). A New Embeddable Reference Electrode for Use in Concrete. *Corrosion*, Paper No. 208, NACE, Houston, TX, USA

[44] Arup, H.; Klinghoffer, O.; Mietz, J. (1997). Long Term Performance of MnO_2–Reference Electrodes in Concrete. *Corrosion*, Paper No. 243, NACE, Houston, TX, USA

[45] Muralidharan S.; Tae-Hyun, H.; Jeong-Hyo, B., et al. (2006). Electrochemical Studies on the Solid Embeddable Reference Sensors for Corrosion Monitoring in Concrete Structure. *Materials Letters*, Vol. 60, pp.651–655

[46] Muralidharan, S.; Tae Hyun Ha; Jeong Hyo Bae; Yoon Cheol Ha; Hyun Goo Lee; Dae Kyeong Kim. (2007). A Promising Potential Embeddable Sensor for Corrosion Monitoring Application in Concrete Structures. *Measurement*, Vol. 40, pp.600-606

[47] Muralidharan, S.; Saraswathy, V.; Thangavel, K., et al. (2008). Electrochemical Studies on the Performance Characteristics of Alkaline Solid Embeddable Sensor for Concrete Environments. *Sensors and Actuators B. Chemical*, Vol. 130, pp. 864–870

[48] Duffó, G.S., Farinab, S.B., Giordano, C.M. (2009). Characterization of Solid Embeddable Reference Electrodes for Corrosion Monitoring in Reinforced Concrete Structures. *Electrochimica Acta*, Vol. 54, pp.1010–1020

[49] Castro, P.; Sagüés, A. A.; Moreno, E. I., et al. (1996). Characterization of Activated Titanium Solid Reference Electrodes for Corrosion Testing of Steel in Concrete. *Corrosion*, Vol. 52, No. 8, pp. 609–617

[50] Muralidharan, S.; Saraswathy, V.; John Berchmans, L., et al. (2010). Nickel Ferrite ($NiFe_2O_4$): A Possible Candidate Material as Reference Electrode for Corrosion Monitoring of Steel in Concrete Environments. *Sensors and Actuators B. Chemical*, Vo.145, pp. 225–231

[51] Myrdal, R. (2007). The Electrochemistry and Characteristics of Embeddable Reference Electrodes for Concrete. *European Federation of Corrosion Publications*, No. 43, Woodhead Publishing Limited and CRC Press LLC. Institute of Materials, Minerals & Mining

[52] John P. Broomfield; Kevin Davies; Karel Hladky. (2002). The Use of Permanent Corrosion Monitoring in New and Existing Reinforced Concrete Structures. *Cement & Concrete Composites*, Vol. 24, pp. 27–34

[53] Gustavo S. Duffó; Silvia B. Farina. (2009). Development of an Embeddable Sensor to Monitor the Corrosion Process of New and Existing Reinforced Concrete Structures. *Construction and Building Materials*, Vol. 23, pp.2746–2751

[54] C. P. Atkins; M. A. Carter; J. D. Scantlebury. (2001). Sources of Error in Using Silver/Silver Chloride Electrodes to Monitor Chloride Activity in Concrete. *Cement and Concrete Research*, Vol. 31, pp.1207-1211

[55] Guofu Qiao; Huigang Xiao; Yi Hong; Yuelan Qiu. (2011). Preparation and Characterization of the Solid-State Ag/AgCl Reference Electrode for RC Structures. *Sensor Review*. (Revised)

[56] Guofu Qiao; Tiejun Liu; Yi Hong; Jinping Ou. (2011) Optimization Design of a Corrosion Monitoring Sensor by FEM for RC Structures. *IEEE Sensor Journal*. DOI:10.1109/JSEN.2011.2112644

[57] J. P. Ou; H. W. Li. (2003). *SPIE*, Vol.5099, pp. 356-362

[58] Y. Yu; H. W. Li; J. P. Ou. (2004). *The 3rd International Symposium on Instrumentation Science and Technology*, Vol.1, pp.741-748, Xi an

[59] Y. Yu; J. P. Ou. (2006). *High Technique Letter*, Vol.12, pp.358-362

[60] S. Glaser; H. Li; M. Wang, et al. (2007). *Smart Structures & Systems*, Vol. 3, pp. 221-244

[61] Kohvakka Mikko; Hannikainen Marko; Hamalainen, et al. (2003). *IECON Proceedings (Industrial Electronics Conference)*. pp. 1499-1504

[62] Scott Meninger; Jose Oscar Mur-Miranda; Rajeevan Amirtharajah, et al. (2001). *IEEE Transaction on very large scale integration (VLSI) systems*. Vol.9, pp.64-76

[63] Yan Yu; Guofu Qiao; Jinping Ou. (2010). Self-powered Wireless Corrosion Monitoring Sensors and Networks. *IEEE Sensor Journal*, Vol. 10, pp. 1901-1902

[64] Guodong Sun; Guofu Qiao. (2011). Corrosion Monitoring Sensor Networks with Energy Harvesting. *IEEE Sensor Journal*. DOI: 10.1109/JSEN.2010.2100041.

[65] Guofu Qiao; Huigang Xiao; Jinping Ou. (2011). Identification of the Reinforcing Steel's Corrosion State in RC beams Based on Electrochemical Sensor. *Sensor Review*. (In Press)

Planet Earth 2011 - Global Warming Challenges and Opportunities for Policy and Practice

Edited by Prof. Elias Carayannis

ISBN 978-953-307-733-8
Hard cover, 646 pages
Publisher InTech
Published online 30, September, 2011
Published in print edition September, 2011

The failure of the UN climate change summit in Copenhagen in December 2009 to effectively reach a global agreement on emission reduction targets, led many within the developing world to view this as a reversal of the Kyoto Protocol and an attempt by the developed nations to shirk out of their responsibility for climate change. The issue of global warming has been at the top of the political agenda for a number of years and has become even more pressing with the rapid industrialization taking place in China and India. This book looks at the effects of climate change throughout different regions of the world and discusses to what extent cleantech and environmental initiatives such as the destruction of fluorinated greenhouse gases, biofuels, and the role of plant breeding and biotechnology. The book concludes with an insight into the socio-religious impact that global warming has, citing Christianity and Islam.

How to reference

In order to correctly reference this scholarly work, feel free to copy and paste the following:

Guofu Qiao, Tiejun Liu, Guodong Sun, Yi Hong, Baoguo Han, Huigang Xiao, Zhichun Zhang and Jinping Ou (2011). Influence of Global Warming on the RC Structures and Durability Monitoring in Civil Engineering, Planet Earth 2011 - Global Warming Challenges and Opportunities for Policy and Practice, Prof. Elias Carayannis (Ed.), ISBN: 978-953-307-733-8, InTech, Available from: http://www.intechopen.com/books/planet-earth-2011-global-warming-challenges-and-opportunities-for-policy-and-practice/influence-of-global-warming-on-the-rc-structures-and-durability-monitoring-in-civil-engineering

INTECH
open science | open minds

InTech Europe
University Campus STeP Ri
Slavka Krautzeka 83/A
51000 Rijeka, Croatia
Phone: +385 (51) 770 447
Fax: +385 (51) 686 166
www.intechopen.com

InTech China
Unit 405, Office Block, Hotel Equatorial Shanghai
No.65, Yan An Road (West), Shanghai, 200040, China
中国上海市延安西路65号上海国际贵都大饭店办公楼405单元
Phone: +86-21-62489820
Fax: +86-21-62489821

IntechOpen